INVESTIGATION OF RADAR BACKSCATTERING FROM SECOND-YEAR SEA ICE

Guang-tsai Lei, Richard K. Moore
and S. P. Gogineni

Radar Systems and Remote Sensing Laboratory
University of Kansas Center for Research, Inc.
2291 Irving Hill Road
Lawrence, Kansas 66045-2969

RSL Technical Report 3311-7

February 1988

Supported by:

Office of Naval Research
Department of the Navy
800 North Quincy
Arlington VA 22213

and

National Aeronautics and Space Administration
Headquarters
Washington DC 20546

Contract N00014-85-K-0200

TABLE OF CONTENTS

FIGURES

TABLES

ABSTRACT

The Mould Bay experiment was conducted in April 1983, to study scattering properties of second-year ice. Radar backscattering measurements were made at frequencies of 5.2 GHz, 9.6 GHz, 13.6 GHz and 16.6 GHz for vertical polarization, horizontal polarization and cross polarizations, with incidence angles ranging from 15° to 70°. The results indicate that the second-year ice scattering characteristics were different from first-year ice and also different from multiyear ice.

The fading properties of radar signals were studied and compared with the experimental data. The influence of snow cover on sea ice can be evaluated by accounting for the increase in the number of independent samples from snow volume with respect to that for bare ice surface. A technique for calculating the snow depth was established by this principle and a reasonable agreement has been observed. It appears that this is a usable way to measure depth in snow or other snow-like media using a radar.

1.0 INTRODUCTION

Approximately 58% of the earth is covered with water: During the winter season sea ice covers 12% of the earth's waters, which is about 7% of the earth's total surface. Information about the types of the sea ice present and their spatial distribution is important for the analysis of global weather patterns and for understanding the interaction between ocean, ice and atmosphere. Furthermore, information about sea-ice formation, drift, and disintegration is essential for resource exploration in ice-covered water and for successful navigation in the Arctic and Antarctic.

Radar remote sensing has great potential in monitoring sea ice. Remote sensing systems operate at wavelengths from high-frequency radio waves up to X-rays. Optical remote sensing is a fairly mature technique and many systems are operational. However, the utility of optical sensors for monitoring of polar regions is limited because these areas are cloud-covered and dark a significant part of the year. Because of their ability to see through clouds and in darkness, microwave radars have developed into powerful tools for the study of sea ice.

Radar backscattering from any target depends both on sensor characteristics and target properties. The sensor parameters of importance are frequency, polarization, antenna beamwidths and incidence angle. The primary target parameters influencing radar return are dielectric constant, surface roughness and internal structure.

The development of radar as a tool for global ice monitoring involves two basic steps: first, selection of radar parameters which are optimized to maximize radar response to certain desired ice characteristics and minimize the dependence on others; second, development of algorithms for interpreting radar data and extracting useful information from the data. A radar image is a pictorial representation of backscattered intensity. Thus an accurate knowledge of ice scattering properties is required both for selecting an optimum sensor and for extracting maximum information from a radar image. Such knowledge is not only a key to automated image interpretation, but also to enhance human interpretation techniques [Holtzman, 1987].

Several field programs were conducted to collect radar data over sea ice during the last few years. Both imaging and non-imaging, and surface-based and airborne sensors were used in these experiments [Gray et al., 1982; Parashar 1974; Onstott et al., 1979; Onstott et al., 1982; Kim, 1984; Gogineni et al., 1984]. However, most of these earlier in situ measurements were on first-year ice and multiyear ice.

In order to measure the backscattering properties of second year ice a joint experiment was conducted by the University of Kansas and Atmospheric Environmental Service (AES), Canada. This experiment was conducted at Mould Bay, N.W.T., Canada during April 1983. The radar measurements were performed by the University of Kansas and surface-comparison measurements were made by the AES.

This project report that summarizes the analysis results of radar data collected during the Mould Bay 83 experiment is organized into six major sections. Section 2 includes a brief review of ice properties and theoretical models applicable to sea ice. Section 3 provides a short summary of the experiment and the system used. Section 4 includes discussions on the angular, frequency and polarization behaviors of different types of ice. Section 5 presents a new method for estimating snow depth from backscatter data. General conclusions about this data set are given in Section 6.

2.0 BACKGROUND

The purpose of this section is to very briefly review ice properties and theoretical models pertinent to understanding scattering properties of sea ice.

2.1 Sea Ice

The radar backscattering from sea ice depends on its physical and electrical properties. The ice parameters of importance to radar remote sensing of sea ice are: surface roughness, dielectric constant and internal structure. These depend on ice age or thickness.

Sea ice can broadly be divided into the following classes according to age and physical properties [WMO, 1970]:

1. New Ice
2. Nilas
3. Pancake Ice
4. Young Ice
5. First-year Ice
6. Old Ice (which is further sub-divided into second-year ice and multiyear ice)

First-year ice (30-180 cm thick) is generally thinner and weaker than multiyear ice (180-360 cm thick). Both types of ice have a rough surface that may be covered with snow. Old ice usually has a rougher surface than that of first-year ice, but it is not so dense as first-year ice because multiyear ice contains many air bubbles in the layer adjacent to the ice surface. This occurs due to the formation of a recrystallized snow layer between the top snow layer and the ice. Moreover, the brine entrapped at the time of freezing drains down in the ice and is replaced by air. Hence, the multiyear ice contains less brine than first-year ice.

2.2 Theoretical Models

The backscattering from sea-ice has been considered to contain two components: surface scattering and volume scattering, which might come from any inclusions in the ice, such as air bubbles or brine pockets, and from snow cover. The popular models for the two components are discussed briefly as follows.

2.2.1 Surface-Scattering Models

When the penetration depth in ice is very small or when the snow cover on the ice surface is wet, the surface scattering can be considered dominant. Several existing models are suitable for explaining the experimental data dominated by surface scattering. These are the physical-optics model (Kirchhoff approximation), small-perturbation method and the two-scale model [Ulaby, Moore and Fung, 1982]. The first one assumes that the radius of curvature at any point on the surface is larger than the incident wavelength.

Hence, the fields on the surface can be approximated by the field on the tangential plane at that point. This theory is applicable at small incidence angles because the surface can be assumed to have large-scale roughness [Fung and Chen, 1971]. Kim [1984] has shown that the physical-optics model using an exponential correlation function can predict the frequency behavior of σ° for first-year ice even well away from vertical (the data used were at angles between 35° and 45°).

The theory of small perturbation is applied for a slightly rough surfaces. The basic idea of this method is to use the plane-wave expansion representation to determine the unknown amplitudes of the scattered fields. Since the amplitude of surface roughness is assumed small (compared with the incident wavelength), the unknown amplitudes may be expanded into a perturbation series in terms of the surface height. Imposing the boundary conditions and the divergence relations, the unknown field amplitudes can be found according to different perturbation orders. For like-polarization scattering, the first-order perturbation is acceptable; while for cross-polarization scattering, the second-order perturbation solution must be used [Valenzuela, 1967; Fung, 1967].

In the two-scale model the natural surface is considered to be given by small-scale roughness superposed on large-scale roughness. The scattering from such surfaces is dominated by large-scale roughness near vertical ($0° < \theta < 15°$) and at large incidence angles ($\theta > 30°$) by small-scale roughness, which is tilted according to the slope distribution of the large-scale roughness of the surface [Fung and Chan, 1971]. The effect of large-scale roughness at large incidence angles is to change the angle in a local coordinate system, which translates the small-scale scattering into the other coordinate system for the two-scale problems. The two-scale model has been successfully applied to sea-surface problems [Moore and Fung, 1979].

2.2.2 Volume Scattering Models

Volume scattering is apparently the major source of the backscattered power for multiyear ice at high frequencies. Two basic approaches are used to model it. One is the radiative-transfer theory, which assumes that the effect of the phase interference between different field quantities is negligible, thus allowing intensity addition. This theory is based on energy equations and is suitable for sparse media. Another approach to explaining the volume scattering is the field approach. It starts with wave equations and includes all of the multiple scattering and interference.

Eom [1982] applied radiative transfer theory in combination with the physical-optics solution under scalar approximation to explain backscattering from sea ice. Kim [1984] further studied the applicability of the combined rough surface and volume model developed by Fung and Eom [1982] to different types of sea ice. The cross-sections computed using this model were in reasonable agreement with measured data at incidence angles from 0° to 70° for frequencies between 4 and 17 GHz.

Most previous work on the application of the field approach to volume scattering from random media is on scattering from sparse media. Foldy's approximation, also called the effective-field approximation (EFA), has been applied to this case [Foldy, 1945].

For dense media, the quasicrystalline approximation (QCA) and the coherent potential approximation (CPA) have been used [Tsang and Kong, 1980; 1982]. The effective-medium approximation (EMA) [Roth, 1974] was developed from the QCA and the CPA. The EMA is more complete than the QCA in that it contains backscattering diagrams and high-order correlation terms [Zhu, 1987]. This method is applied to solve for the randomly distributed dense discrete scatterers from half spaces under the condition of spherical scatterers and a planar boundary. This model compares well with experimental data for all angular regions (0°-90°) and indicates that the ratio of polarized to depolarized backscattering cross-section is equal to 8 [Zhu, Fung and Wong, 1987].

2.3 Empirical Model

Radar backscatter from terrain is known as "clutter" to designers of radars looking for "hard targets." An empirical "clutter model" was developed by Moore [1979] for average radar backscatter from snow-covered ground and sea

ice. Since it is an average, it applies directly to radars whose resolution cell is large enough to average many individual elements. The model takes the form

$$\sigma^\circ \text{ (dB)} = A + B\theta + CF + DF\theta \qquad 20^\circ < O < 70^\circ$$

$$\text{for} \quad 1\text{GHz} < f < 18\text{GHz}$$

where A, B, C, and D are constants.

The model is also presented for angles of incidence of 10° to 0° in the form

$$\sigma^\circ \text{ (dB)} = M(\theta) + N(\theta)f \qquad \text{for} \quad 1 \text{ GHz} < f < 18\text{GHz}$$

The land version of this model is based on regression of data obtained since 1974 and hundreds of thousands of data from the University of Kansas microwave active spectrometers and Skylab S-193. Surprisingly, this simple model gives variations quite close to those from the computation-intensive theoretical models. The sea-ice version is based on early (prior to 1979) University of Kansas and CCRS measurements.

3.0 EXPERIMENT AND SYSTEM DESCRIPTIONS

3.1 Experiment

This experiment consisted both of radar measurements and surface observations. Radar data were acquired with a sled-mounted scatterometer called SLEDSCAT. The radar was mounted on a sled which was pulled by a tracked vehicle. The data were collected at selected frequencies between 4 and 17 GHz with the like and cross antenna polarizations for incidence from 15 to 70 degrees.

The radar data were collected to meet two basic interrelated objectives: first, to study the ability of radar to discriminate second-year ice from first-year ice; and second, to test the radar's ability to identify various sub-categories of ice. The basic approach adopted for data collection during this experiment was to obtain full-length profiles of selected study sites. This was done at 5.3, 13.6 and 16.6 GHz with VV-polarization at an incidence angle of 50 degrees. The data were extended to cover as many other angles, frequencies and polarizations as possible.

The surface measurements consisted of qualitative descriptions of snow and ice characteristics, salinity, temperature, snow depth and other environmental variables.

The ice types studied in this experiment were: lake ice, bare and snow-covered first-year ice, and second-year ice. The thickness of the first-year ice varied between 0.2 and 2m, and of second-year ice ranged from about 1.8 to 4 m. During the period of this experiment, the second-year ice surface was relatively smooth. On the first-year ice the average depth of snow was less than about 5 cm.

3.2 System

The SLEDSCAT is a frequency-modulated continuous-wave radar that operates from 4 GHz to 18 GHz, over incidence angles from vertical to 80 degrees and with both like and cross antenna polarizations. Relative calibration of the system was performed by measuring a sample of the transmitted signal passed through a delay line of known loss. The relative measurements were converted to absolute values by comparing them (at less-frequent intervals) with the power obtained from a Luneberg-lens reflector of known radar cross-section. System specifications are given in Table 3.1. Two-way 3-dB antenna beamwidths are given in Table 3.2.

TABLE 3.1 System Specifications

(C-X-Ku-Band)

TYPE	FM-CW
Frequency Range	4-18 GHz
Modulation	Triangle
FM Sweep Bandwidth	600 MHz
Transmitter Power	10-19 dBm
Intermediate Frequency	14.5 kHz
IF Bandwidth	3.5 kHz
Antennas:	
Receive Type	Standard Gain 4-6 GHz Horn
	8-18 GHz Horn-fed Parabolic Dish
Transmit Type	Standard Gain 4-6, 8-12 and 12-18 GHz Horns
Polarization Capabilities	HH, VV and CROSS
Target Distance	3-7 meters
Transmit Beamwidth	(See table 4-2)
Receive Beamwidth	(See table 4-2)
Incidence Angle Range	10° - 70°
Calibration:	
Internal	Signal Injection (delay line)
External	Luneberg Sphere (reflector)

TABLE 3.2 Antenna Beamwidth

FREQUENCY		5.3	9.6	13.6	16.6
VV	(AZ)	16.2	7.6	6.2	5.2
	(EL)	16.2	6.3	5.7	4.3
HH	(AZ)	16.2	6.3	5.7	4.3
	(EL)	16.2	7.6	6.2	5.2
X	(AZ)	17.3	6.3	5.8	7.5
	(EL)	17.3	7.6	6.0	4.9

4.0 EXPERIMENTAL RESULTS

The results of the analysis of data from Mould Bay 83 experiment are presented in this section. First, selected time series plots of received power are presented. Next, angular, frequency, and polarization responses of each type of sea ice are discussed.

4.1 Profiles

Two selected profiles of the return power measured in the experiment are presented in this section. The radar return in each plot is given as a function of time taken to traverse the observed path. Profiles #1 and #2, acquired at an incidence angle of 50° with VV polarization at frequencies 13.6 GHz and 16.6 GHz, are shown in Fig. 4.1. The difference in return for segments R1, R4, and R6 (first-year ice) and R3 (second-year ice) shows that it is possible to separate second-year ice from first-year ice at this angle and these frequencies. An old lead (R4) was embedded in the second-year ice, and both the snow-covered first-year ice and second-year ice were uniformly rough except at the boundary between them.

4.2 Angle Responses

Angular responses of the backscatter from first-year ice and second-year ice are shown in Fig 4.2 a-g. The simple clutter model (exponential variation of σ° with θ) was tested against the data using the chi-square test, and it fits well. The reduced chi-square (chi-square/degrees of freedom) should be approximately equal to one for chi-square tests [Bevington, Chap. 5, 1969]. The results listed in Table 4.1 show that the simple clutter model can predict the angular behavior from first-year ice and second-year ice over the frequency range 5.2 GHz - 16.6 GHz and the angular range 20° - 70°. Only three out of the 24 cases failed the test (values >1), and these by only small amounts.

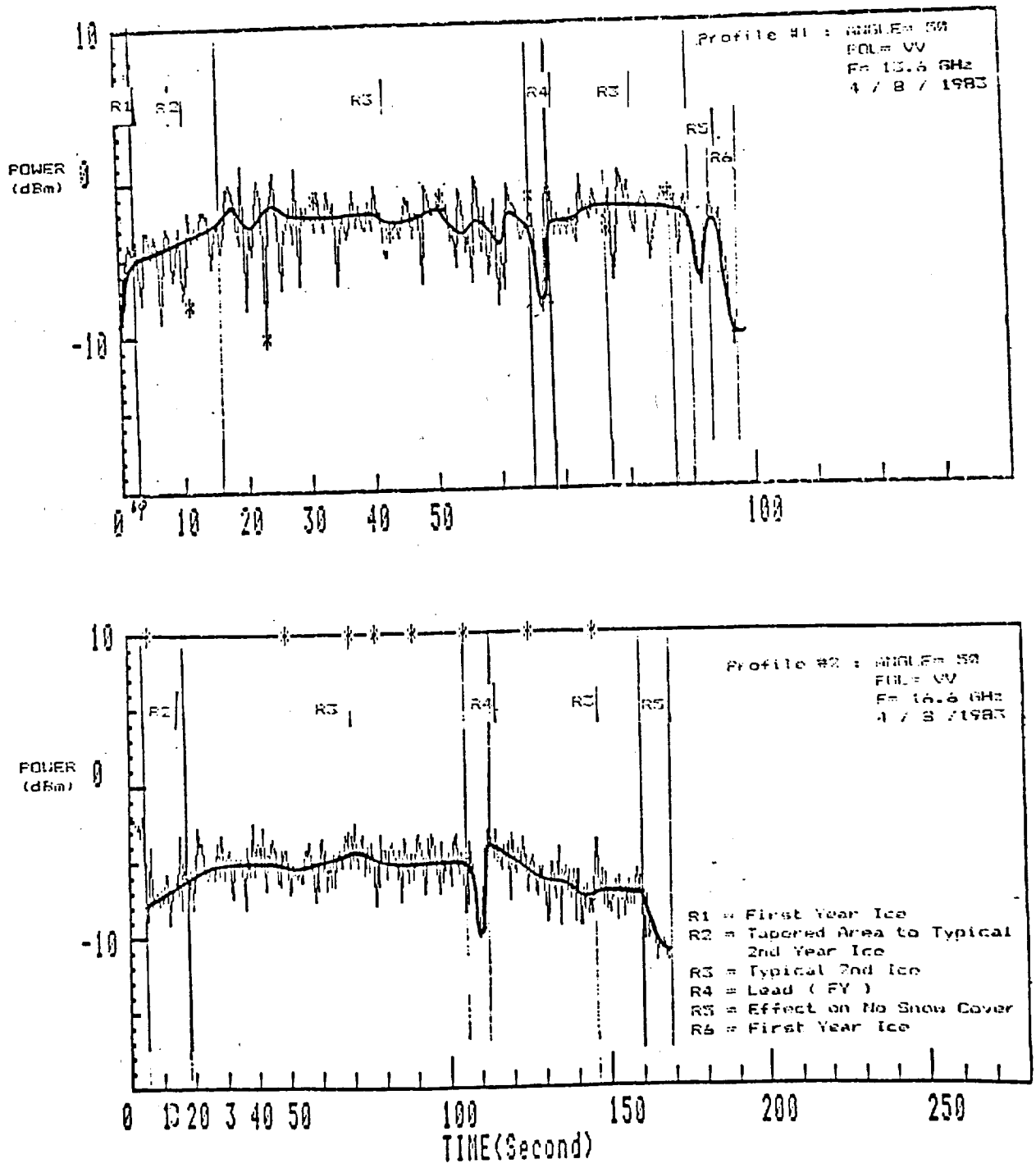

FIGURE 4.1. Profile of a Composite Second-Year Ice

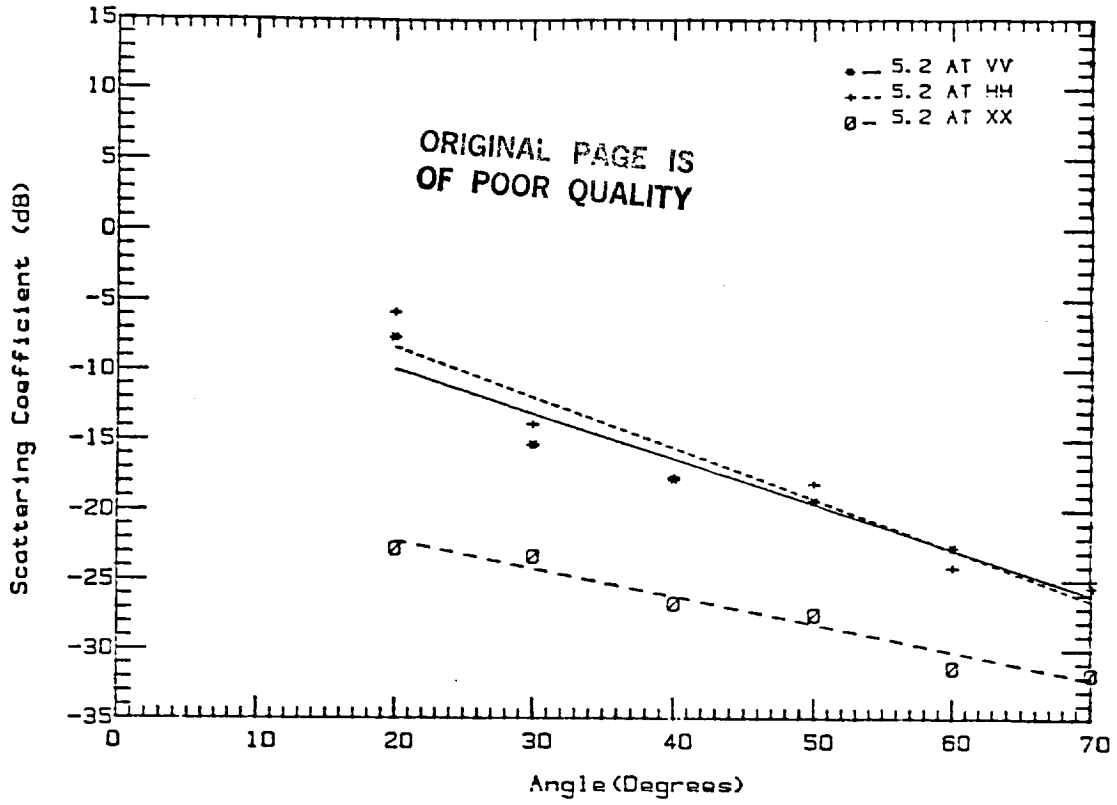

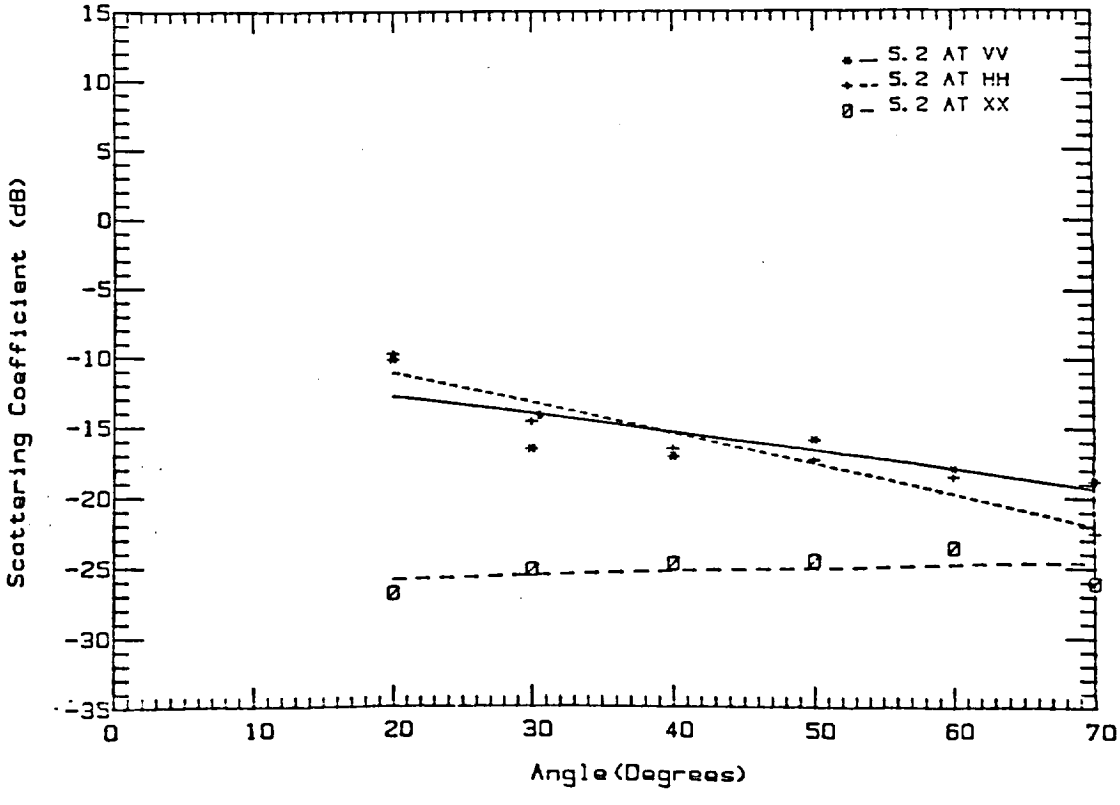

FIGURE 4.2-a. Mould Bay, top Apr. 13, 1983 FYI; bottom Apr. 19, 1983 MYI

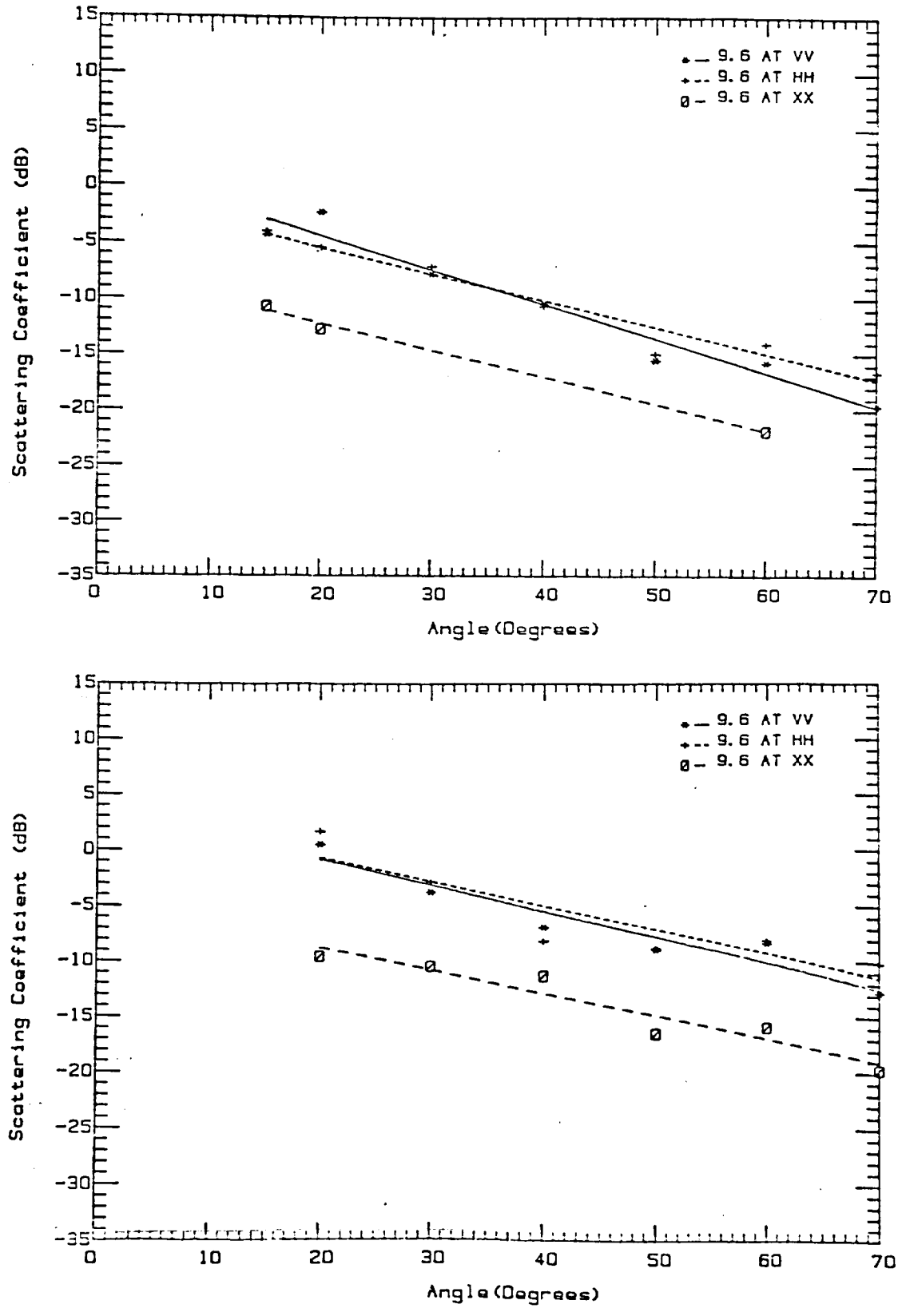

FIGURE 4.2-b. Mould Bay, top Apr. 13, 1983 FYI; bottom Apr. 19, 1983 MYI

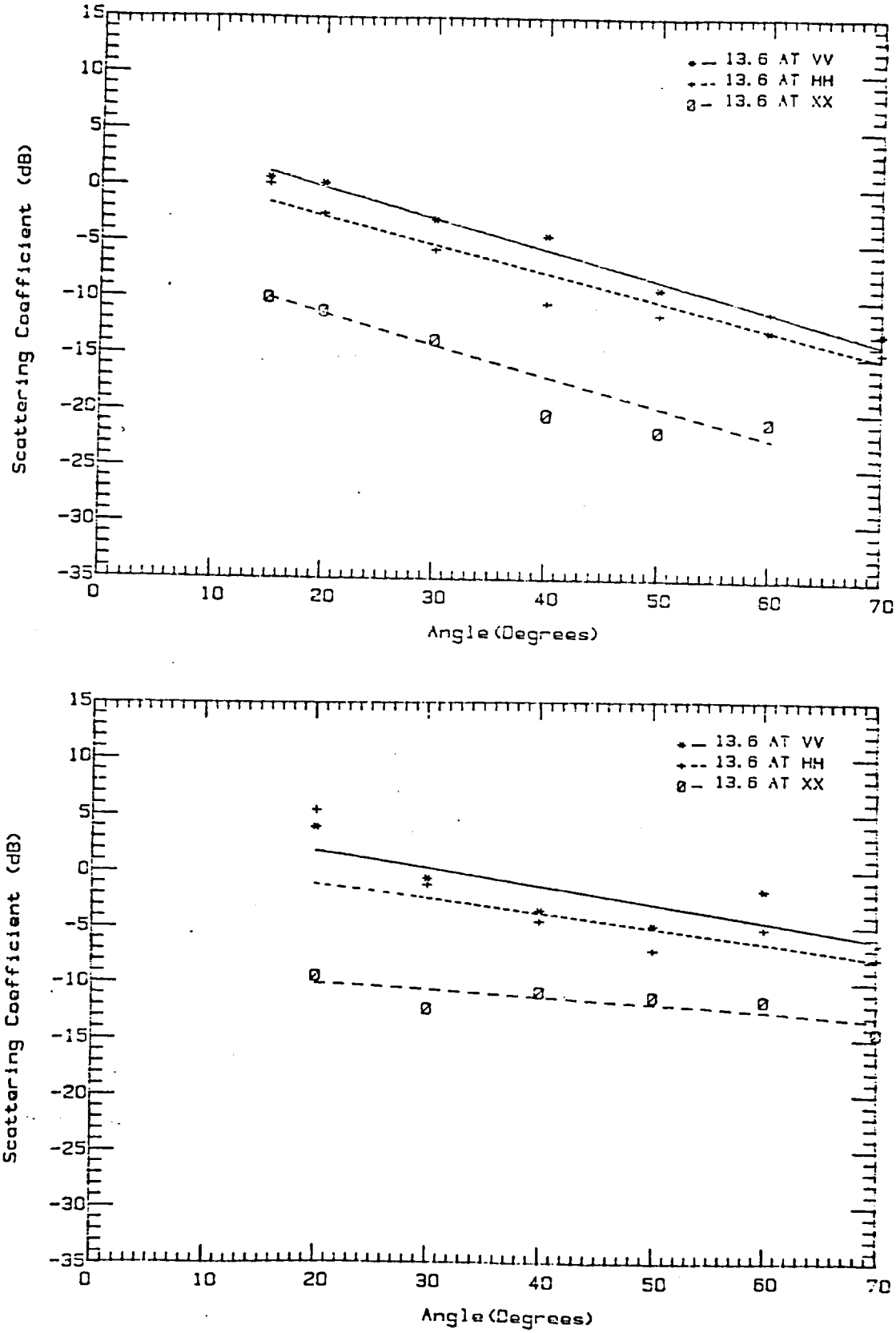

FIGURE 4.2-c. Mould Bay, top Apr. 13, 1983 FYI; bottom Apr. 19, 1983 MYI

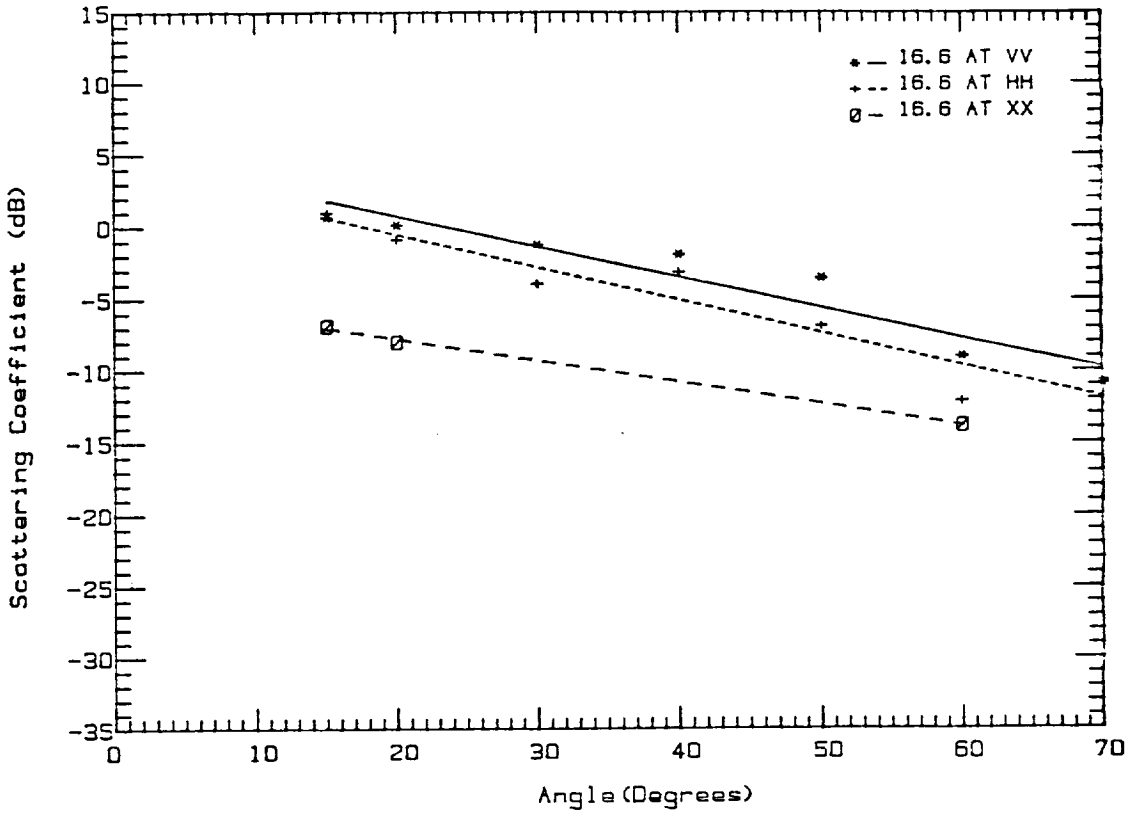

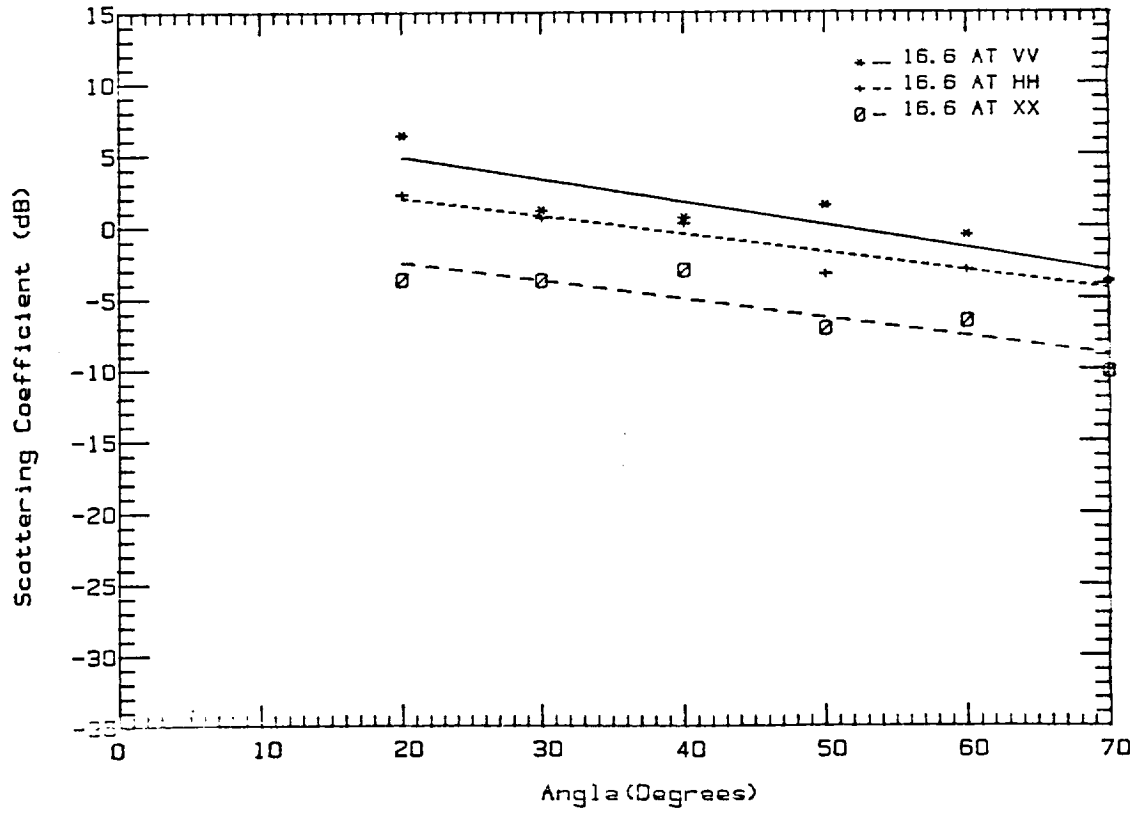

FIGURE 4.2-d. Mould Bay, top Apr. 13, 1983 FYI; bottom Apr. 19, 1983 MYI

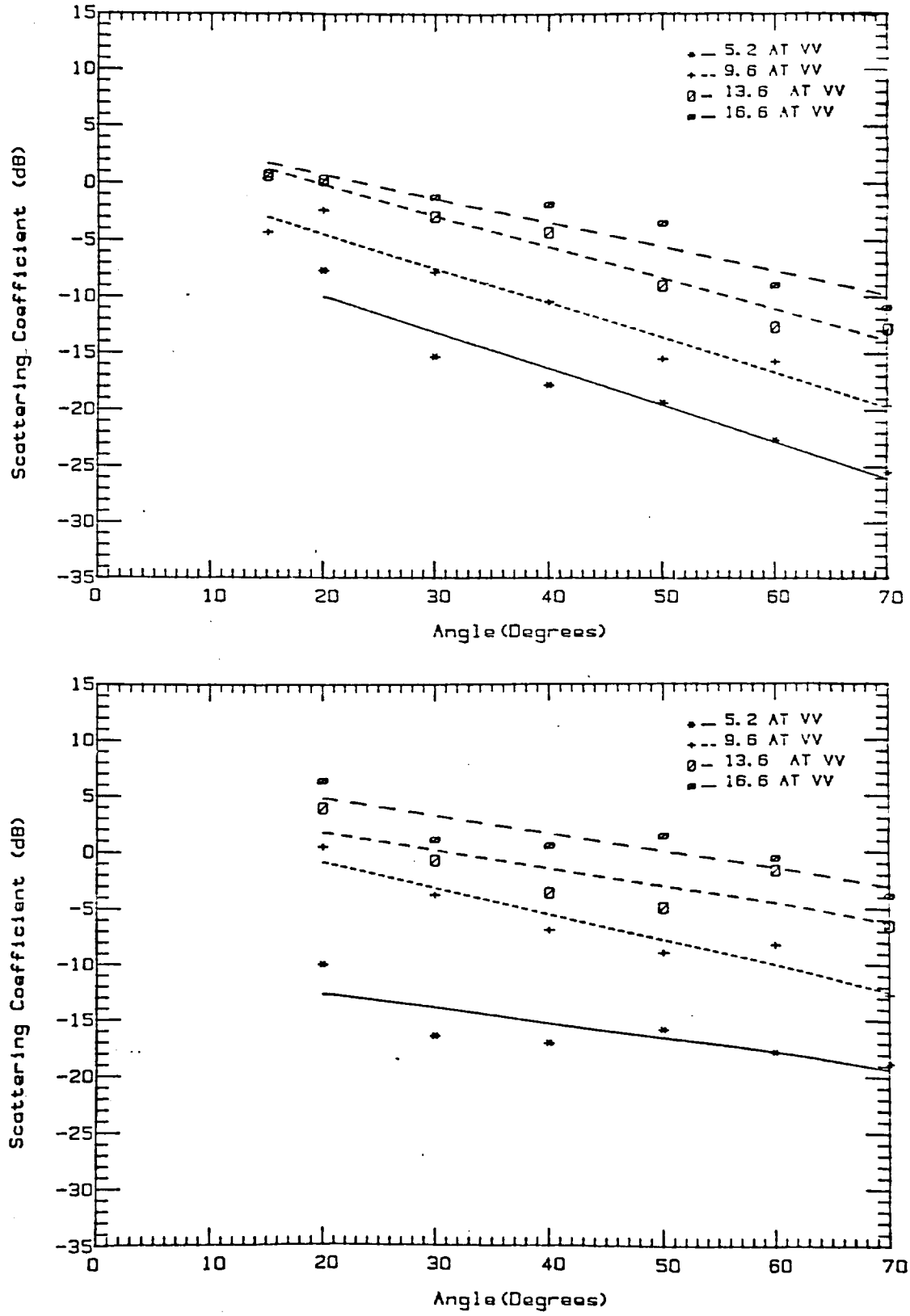

FIGURE 4.2-e. Mould Bay, top Apr. 13, 1983 FYI; bottom Apr. 19, 1983 MYI

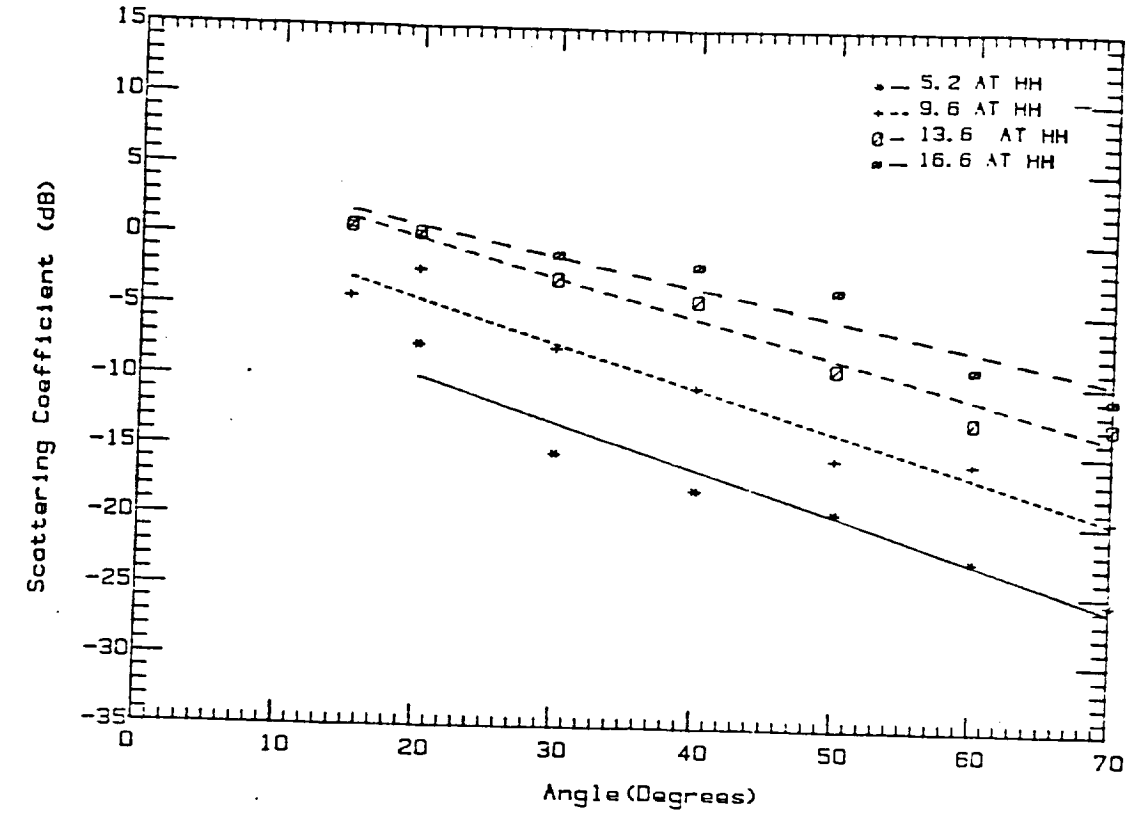

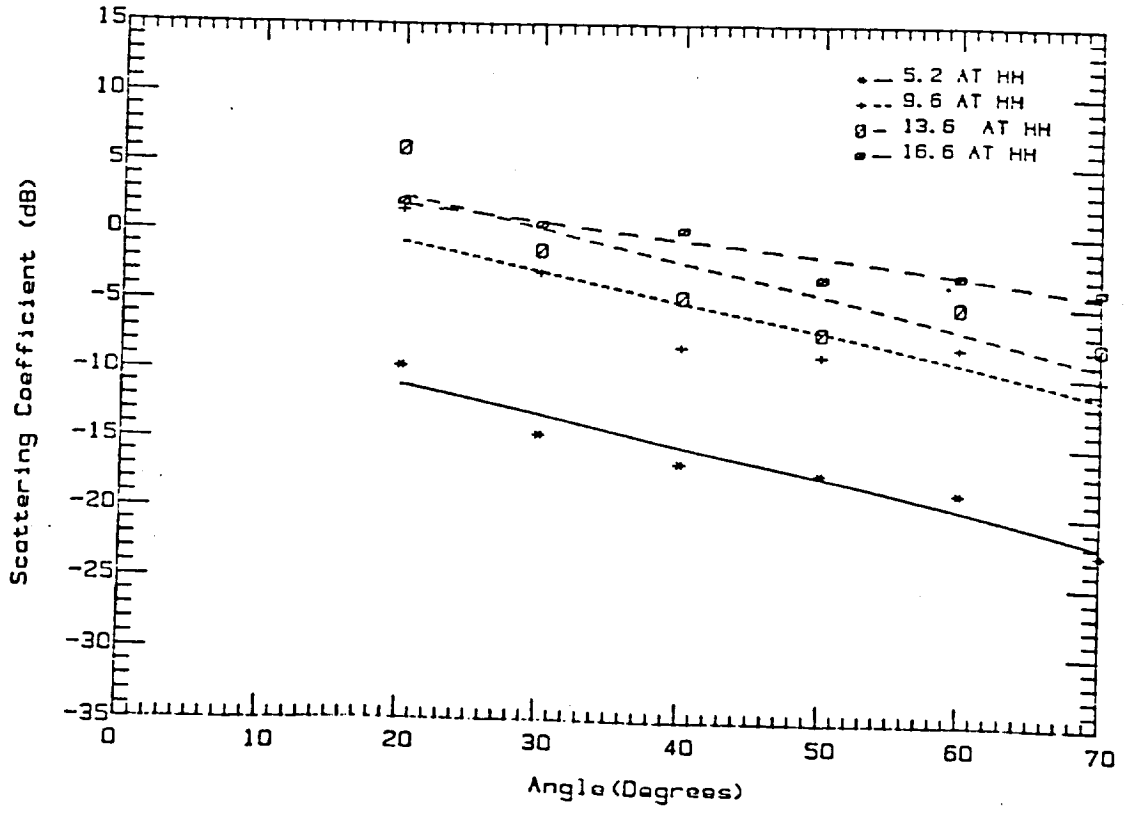

FIGURE 4.2-f. Mould Bay, top Apr. 13, 1983 FYI; bottom Apr. 19, 1983 MYI

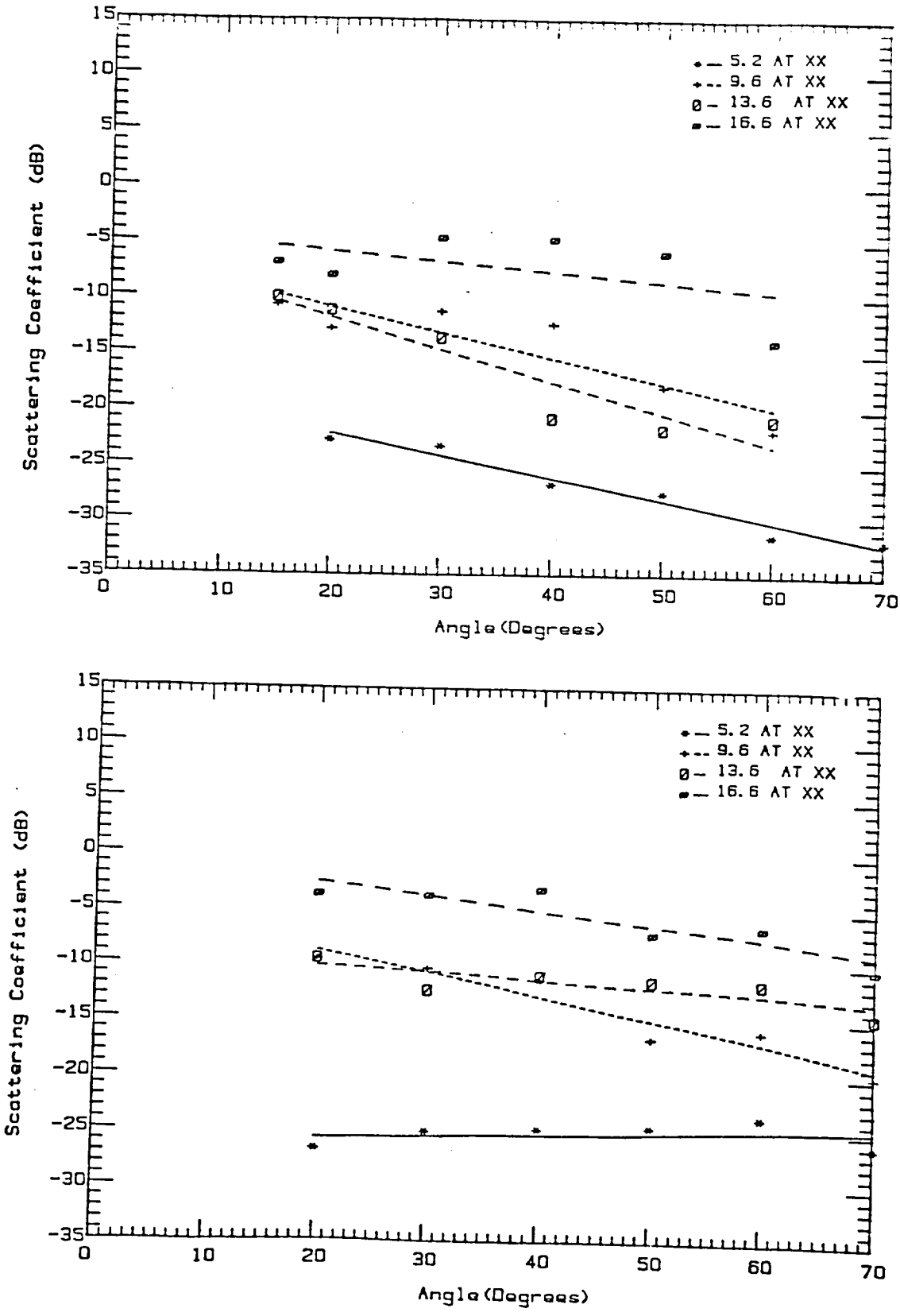

FIGURE 4.2-g. Mould Bay, top Apr. 13, 1983 FYI; bottom Apr. 19, 1983 MYI

TABLE 4.1 Chi-Square/Degree of Freedom
(Fitting Results With The Clutter Model)

FREQ (GHz)	5.2	9.6	13.6	16.6
SYI	1.0	0.7	1.2	0.8
VV FYI	0.9	0.7	0.5	0.7
SYI	0.7	1.2	0.9	0.5
HH FYI	1.1	0.6	0.8	0.7
SYI	0.6	0.7	0.6	0.7
XX FYI	0.5	0.6	0.9	0.3

The σ° of old ice usually decays with angle more slowly that that of new ice, particularly at the higher frequencies. Presumably this occurs because volume scatter from old ice dominates the return at higher frequencies [Kim, 1984]. Table 4.2 shows that the slopes of the angular variation are less in all cases for SY ice than for FY ice, although for some cases the differences are small. Conceivably the smaller differences than observed previously (see Figs. 4.2-h and -i) for multiyear ice are caused by a difference between the incomplete bubble formation of the second-year ice and the more complete formation for the multiyear ice. This agrees with Campbell, et al. [1977], who state that the upper layer of multiyear ice consists of recrystallized ice containing large air bubbles and haveing a density of 0.7-0.8 g/cm^3. These bubbles may not have grown to their full size in SY ice.

Nevertheless, it is clear from both the figures and Table 4.2 that the more rapid fall-off with angle of the FY ice echo means that discrimination between SY and FY is better at higher angles of incidence. No significant difference is apparent between the slopes observed by Kim for MY ice and those observed here for SY ice. However, the levels of 9.6 and 13.6 GHz signals observed here are higher. At this time we cannot explain this difference.

The gentle slopes of the cross-polarized returns suggest that they are largely due to volume scatter. The higher cross-polarized return at 16.6 GHz and lower cross-polarized return at 5.2 GHz (see Fig. 4.2-g) may be due to the increased volume scattering at the higher frequencies where the wavelength is closer to the size of the bubbles.

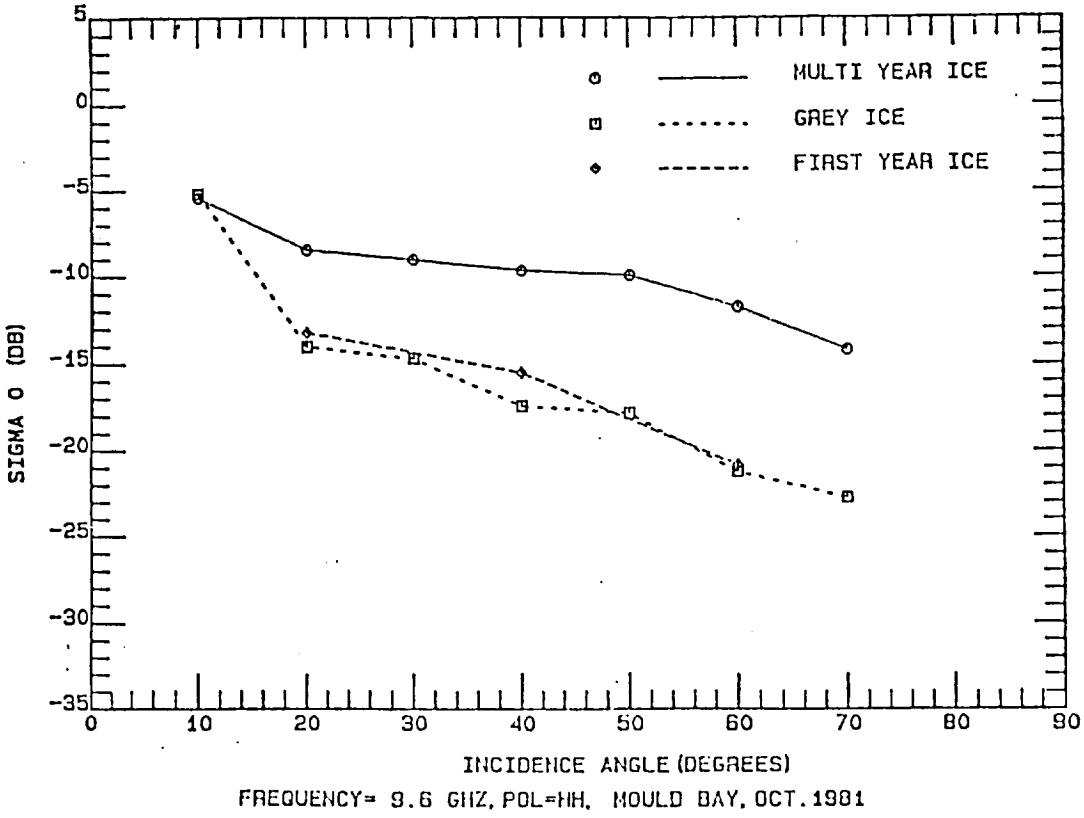

FIGURE 4.2-h. Typical Angular Behavior of Average σ° (From Kim, 1984)

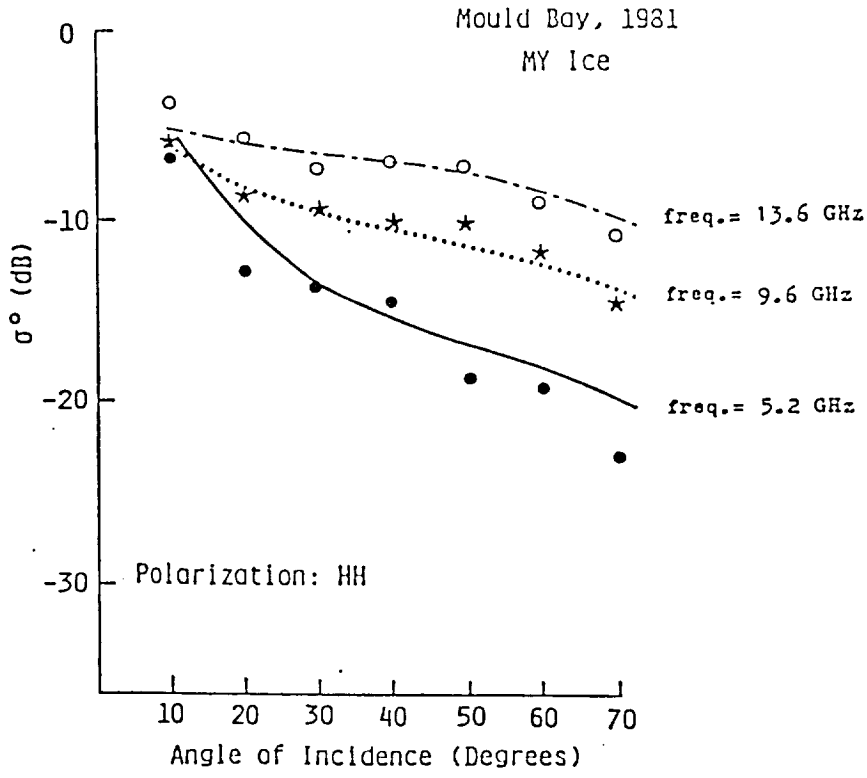

FIGURE 4.2-i. (From Kim, 1984)

TABLE 4.2 Slopes Of The Angular Response Curves

FREQ (GHz)		5.2	9.6	13.6	16.6
VV	SYI	-.14	-.23	-.16	-.16
	FYI	-.32	-.31	-.28	-.21
HH	SYI	-.22	-.22	-.14	-.13
	FYI	-.36	-.24	-.25	-.23
XX	SYI	-.02	-.21	-.07	-.13
	FYI	-.20	-.24	-.27	-.15

4.3 Polarization Behaviors

4.3.1 Like-polarization measurements

At high frequencies (13.6 GHz and 16.6 GHz) σ°_{vv} is slightly higher than σ°_{hh} for both first-year ice and second-year ice. This might indicate that the backscattering was not purely a surface phenomenon for both second-year ice and first-year ice. Due to the Brewster angle effect, the power transmitted into the ice medium is larger for the vertically polarized waves than for the horizontally polarized waves. Thus, if volume scattering is present, σ°_{vv} would be higher than σ°_{hh} if the scatterers are isotropic. At 9.6 GHz and 5.2 GHz, where the effect of volume scattering was weaker σ°_{vv} and σ°_{hh} had very similar cross-sections.

4.3.2 Cross-polarization measurements

The cross-polarization measurements resulted in about a 5-8 dB lower return than like polarizations at large angles ($\theta > 50°$), but the radar cross section was still measurable. Cross-polarization did not offer any additional contrast over like-polarization.

4.4 Frequency behavior

Spectral responses of the backscatter coefficients at selected angles are shown in Fig. 4.4 a-c. The backscatter is generally found to increase linearly with frequency, and first-year ice returns were lower than those from second-year ice. The best contrast was obtained at 60°, and larger angles seem to give better contrast than smaller angles. Comparing Fig. 4.4-d with Fig. 4.4 a-b, we see that the frequency responses of the first-year ice and second-year ice were similar to that of the first-year ice in Mould Bay, October 1981. The effect of the volume scattering is stronger at high frequencies than at lower frequencies and at large incidence angles the contribution due to surface roughness is very small. Hence, for large incidence angles the frequency-response curves should have larger slopes than those for smaller incidence angles if there are enough volume scatterers in the ice. This can be seen clearly for multiyear ice in 1981, but it did not occur for second-year ice in 1983. Again it can be explained that the density of the second-year ice was too high or not enough inclusions in the second-year ice contributed to the return power.

Kim [1984] showed (see Fig. 4.4-e) that the (raw) depolarization ratio ($\sigma°hh/\sigma°hv$) decreases with frequency at the incidence angles of 22° and 35°. Now, comparing Fig. 4.4-f with Figure 4.4-g, -h and Fig. 4.4-i with Fig. 4.4-j, it can be noted that at small incidence angles such as 40° and 20° this is true, but at large incidence angles such as 60° and 70°, where the surface roughness plays a small role, the depolarization ratio was almost constant and independent of the frequency. If corrections are made for non-planar boundary and non-spherical scatterer shape, the difference between the two like-polarized curves and the cross-polarized curve will possibly be 9 dB (equal to 8). It seems that the depolarization ratio for volume scattering is indeed a constant that is independent of the angle, frequency and ice types, as indicated theoretically by Zhu, et al., (1987).

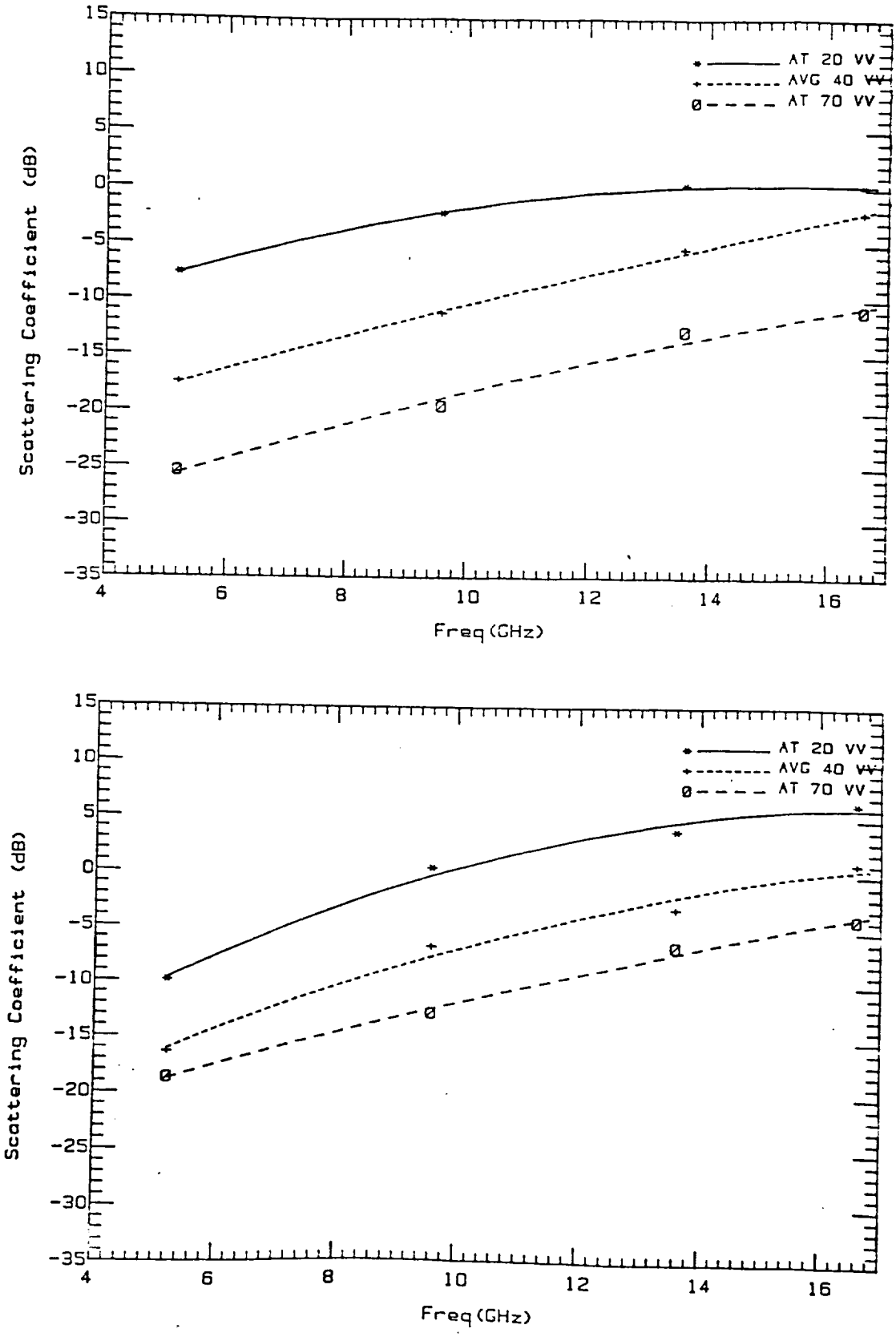

FIGURE 4.4-a. Mould Bay, top Apr. 13, 1983 FYI; bottom Apr. 19, 1983 MYI

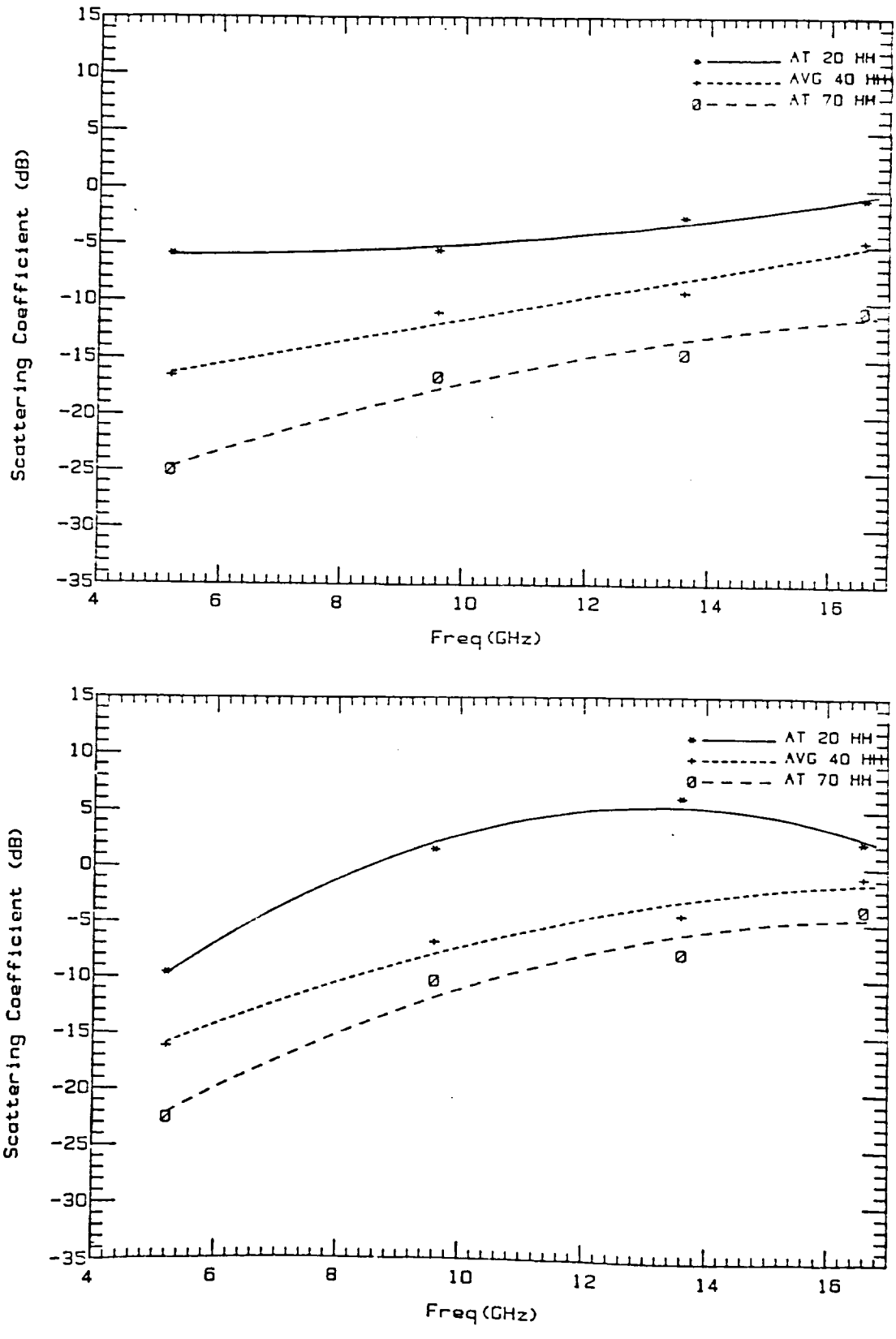

FIGURE 4.4-b. Mould Bay, top Apr. 13, 1983 FYI; bottom Apr. 19, 1983 SYI

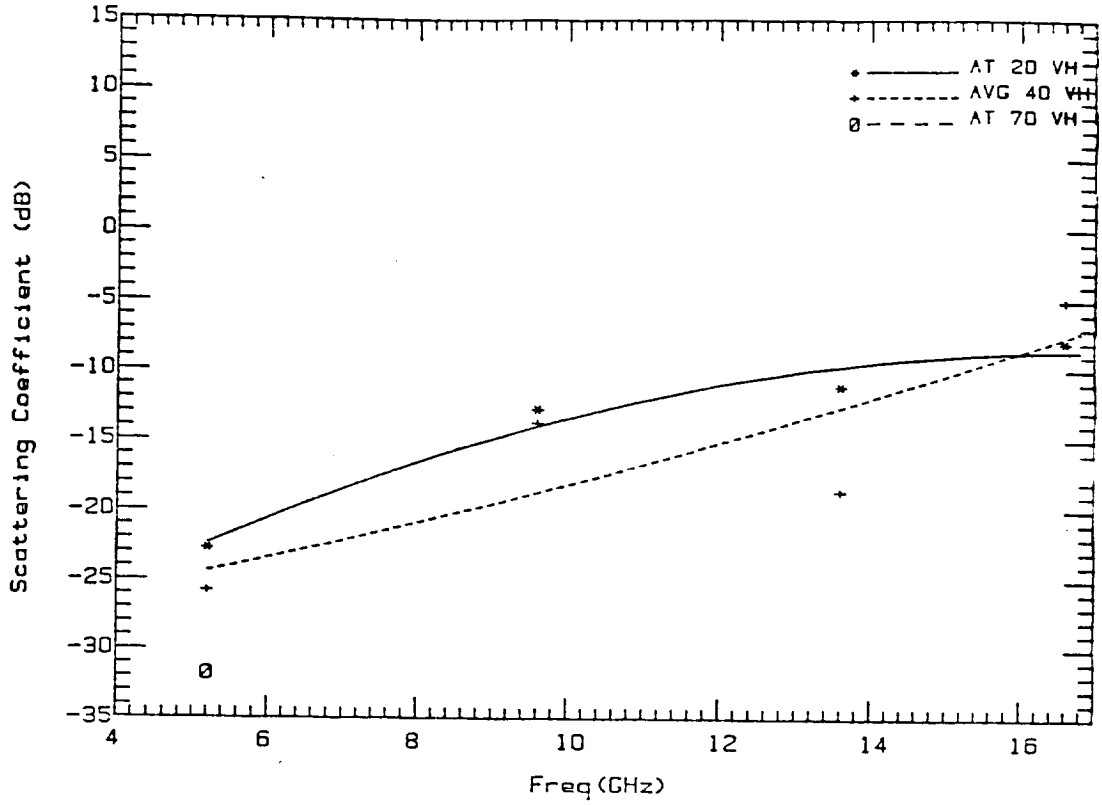

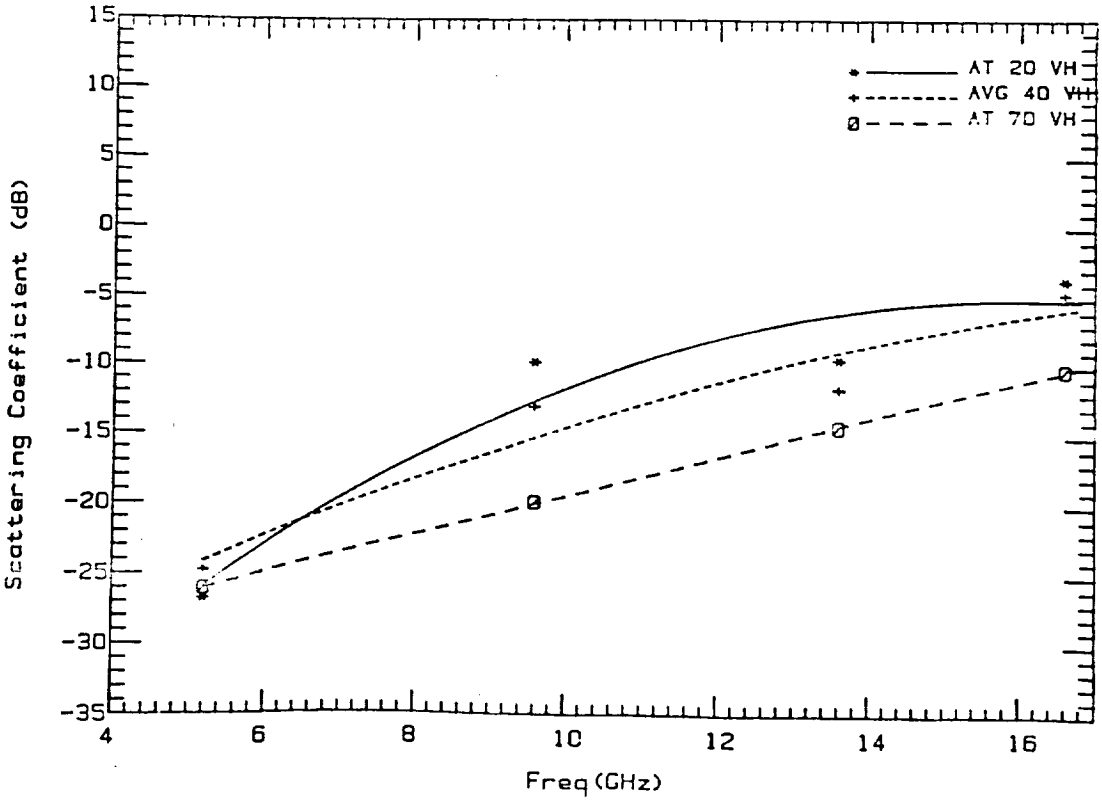

FIGURE 4.4-c. Mould Bay, top Apr. 13, 1983 FYI; bottom Apr. 19, 1983 SYI

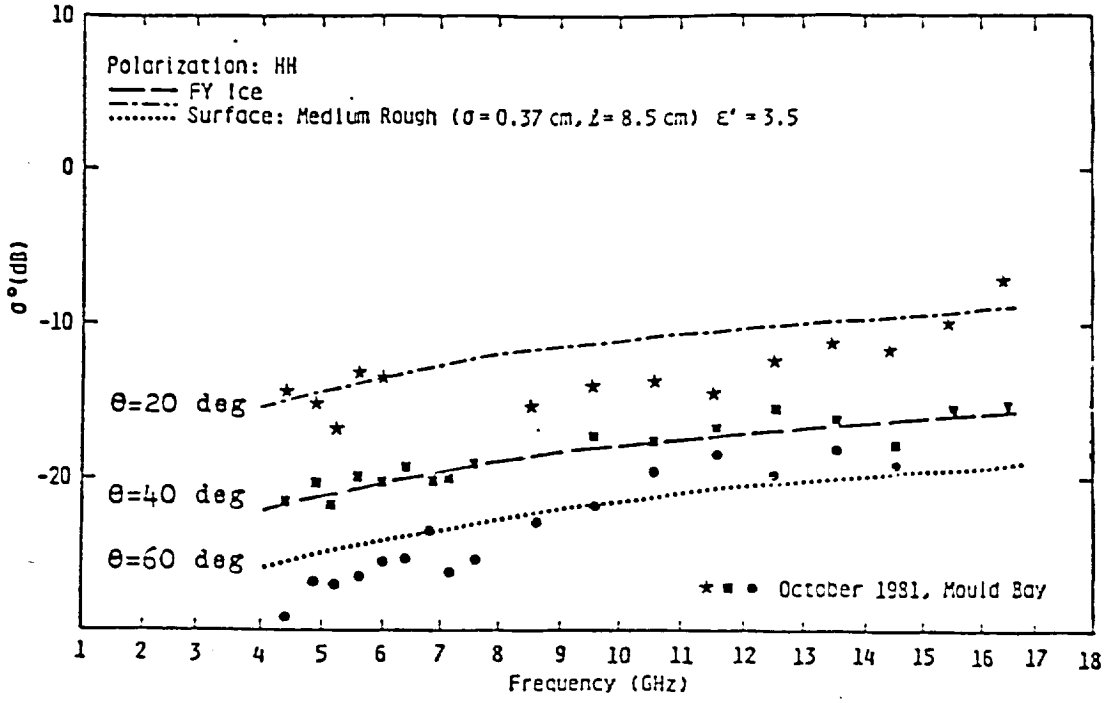

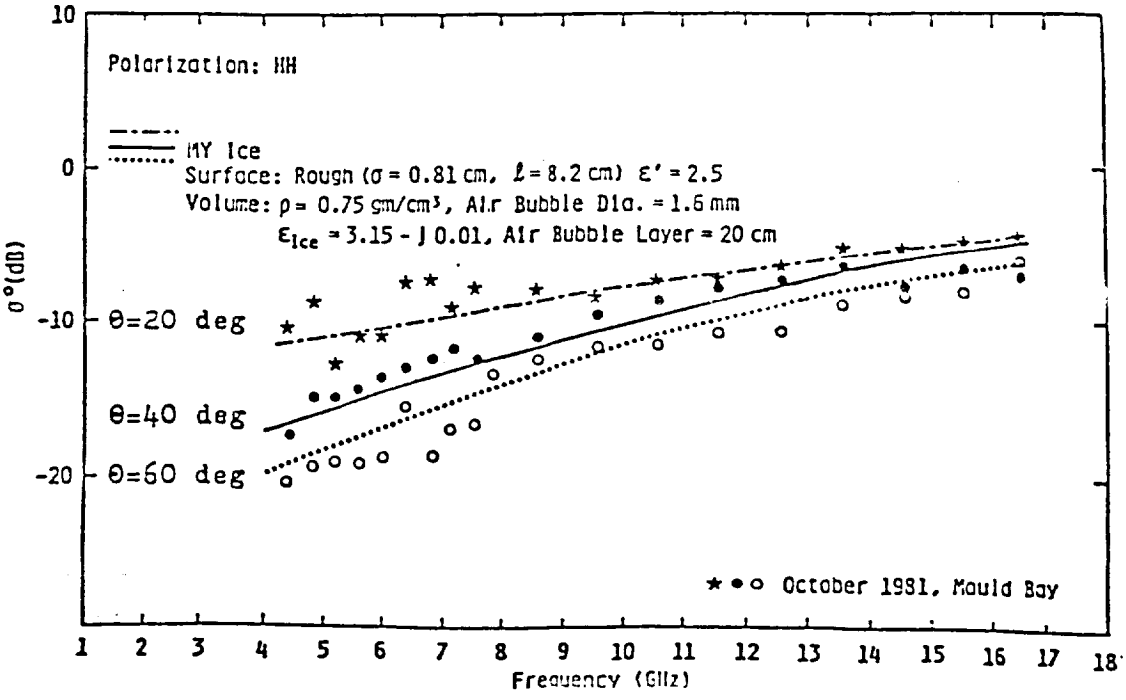

FIGURE 4.4-d. (From Kim, 1984)

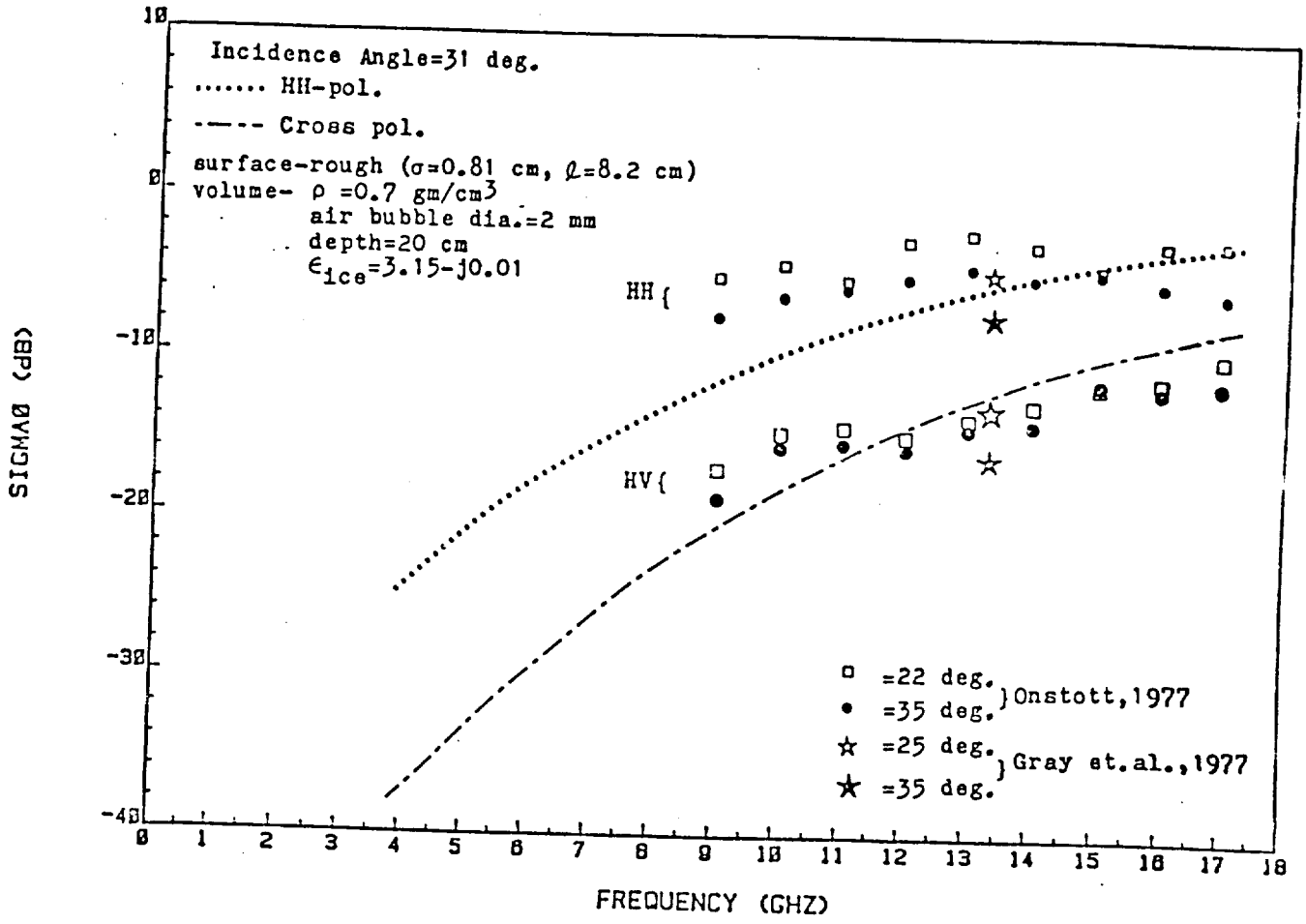

FIGURE 4.4-e. Theoretical Volume Scattering Backscattering Coefficient of Multiyear Ice with Rough Surface. Like- and cross-polarized cases are calculated and compared with measurements, although the pure surface-scattering term is not included in calculations. (From Kim, 1984)

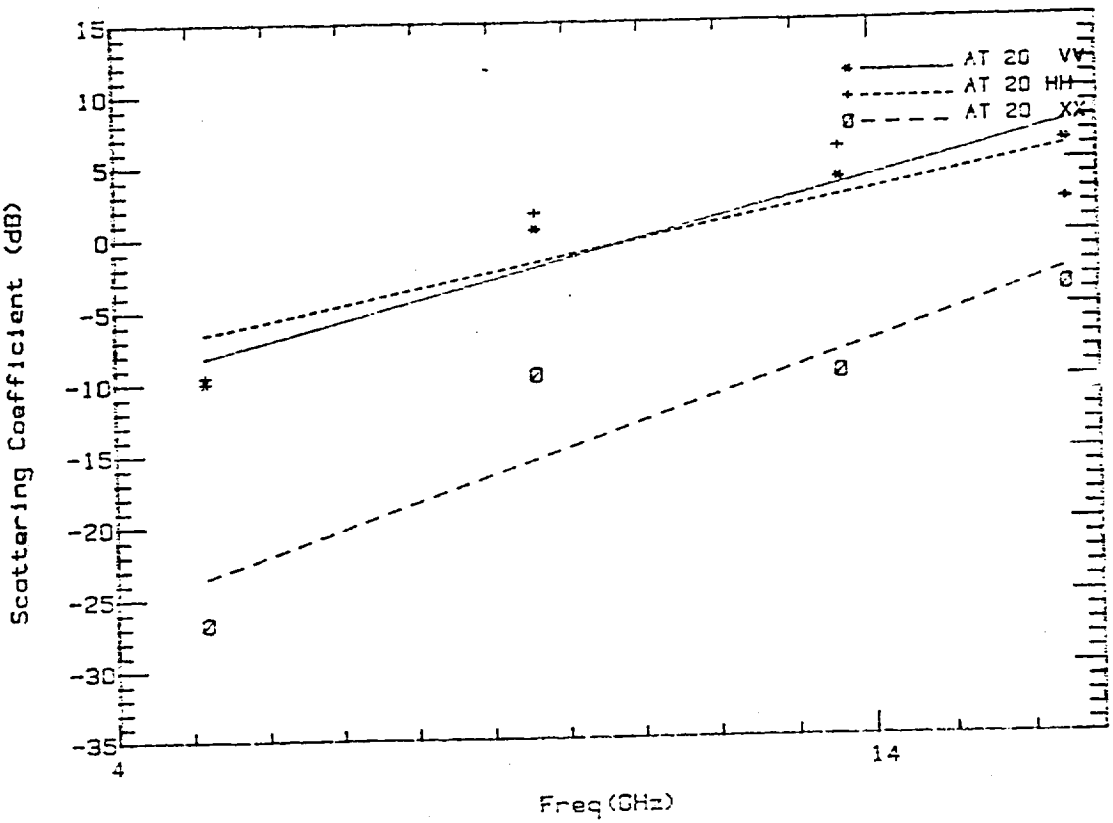

FIGURE 4.4-f. Second-Year Ice

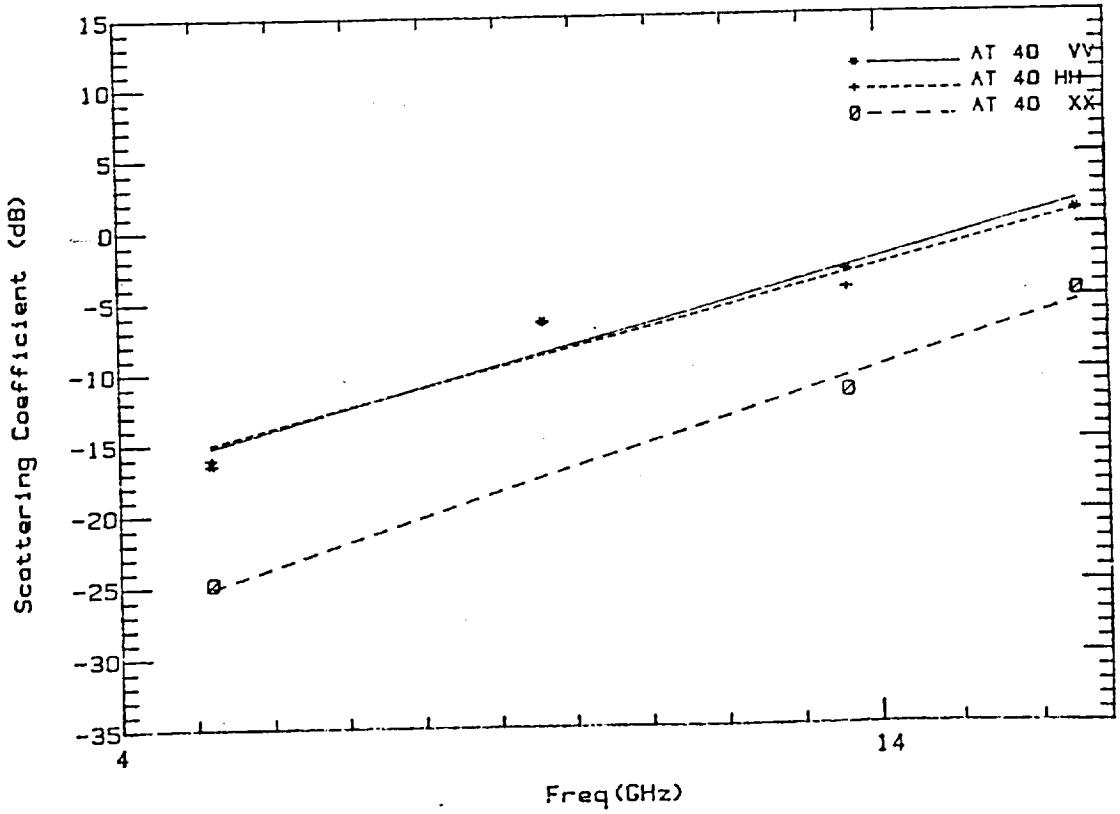

FIGURE 4.4-g. Second-Year Ice

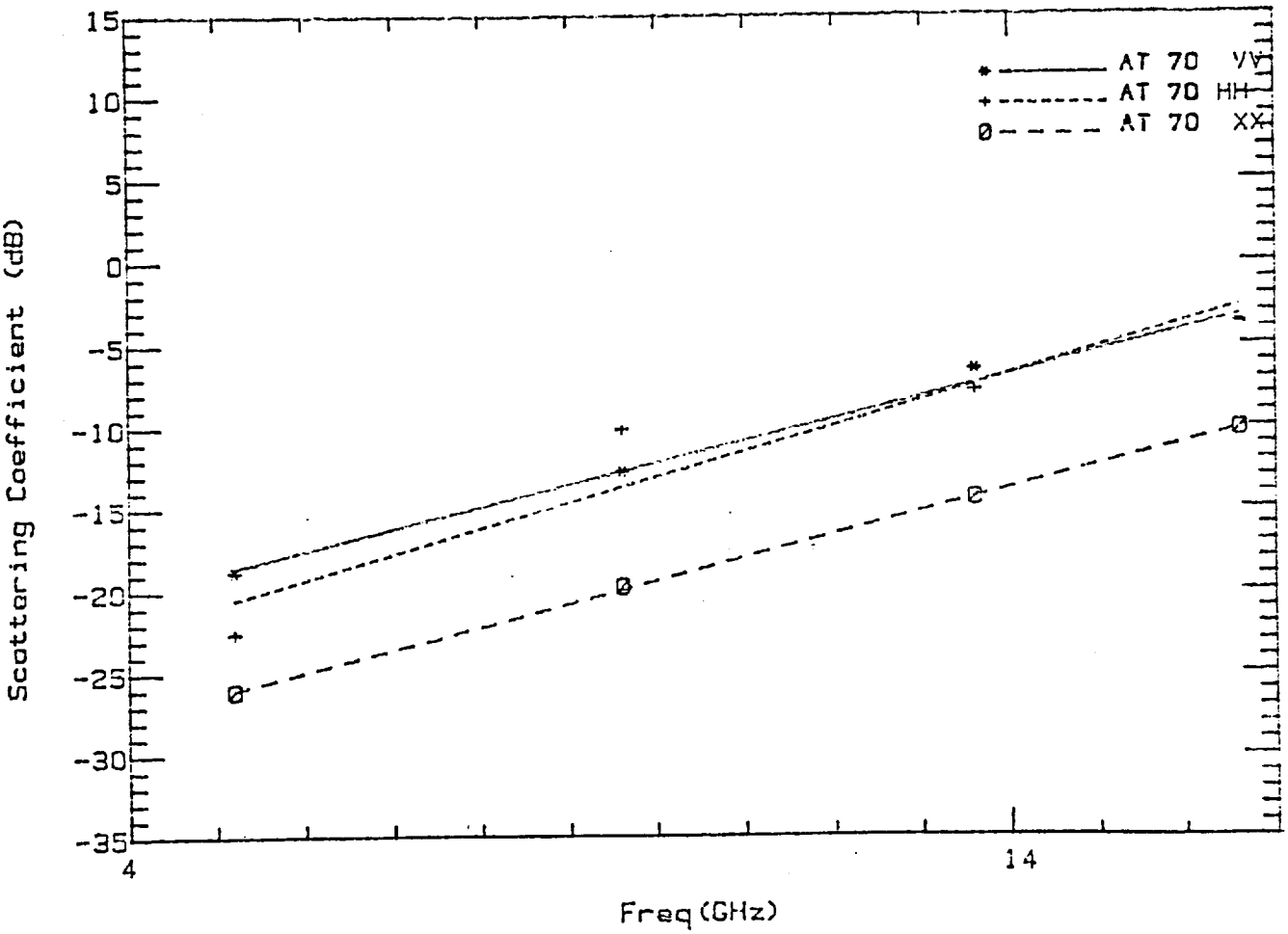

FIGURE 4.4-h. Second-Year Ice

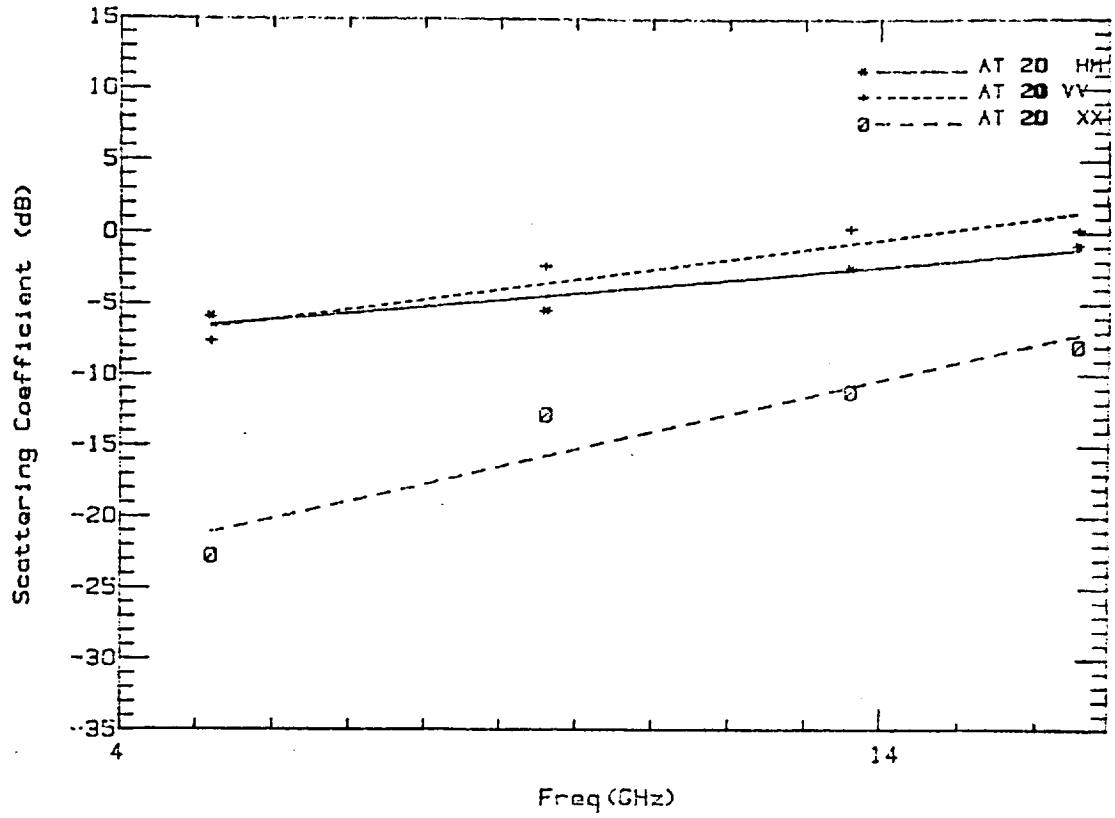

4.4-i. First-Year Ice

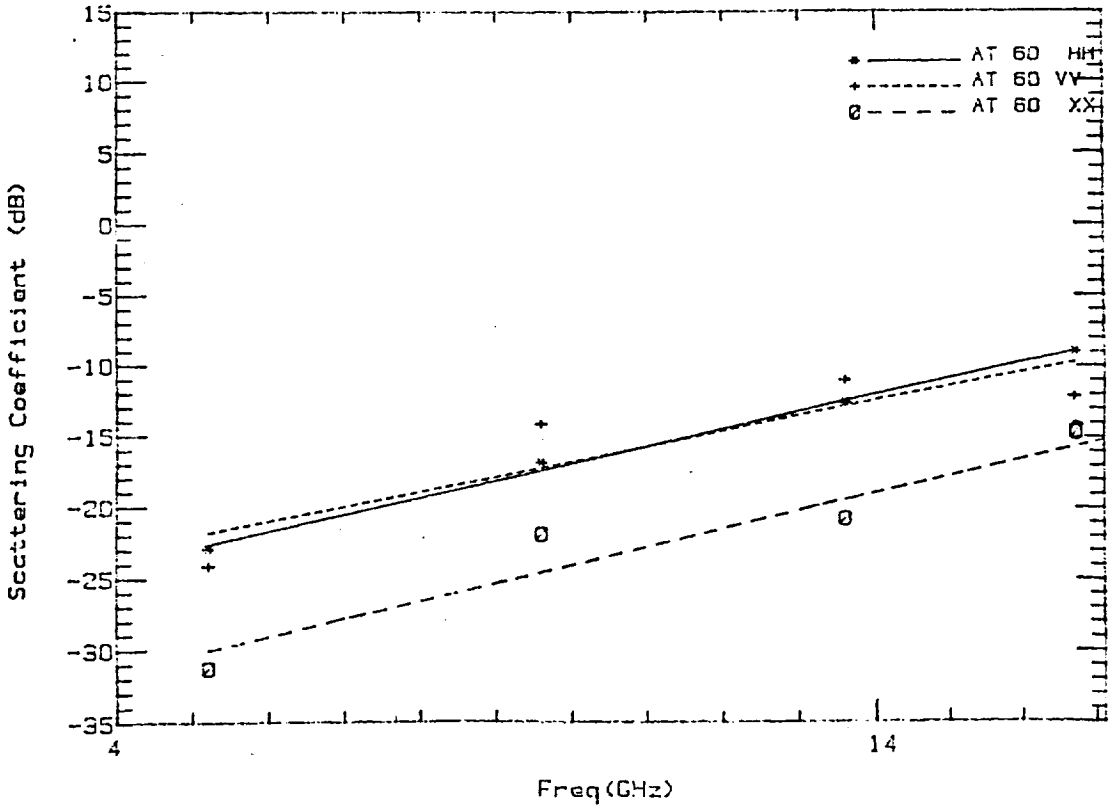

FIGURE 4.4-j. First-Year Ice

4.5 Contrast of σ° between different ice types

4.5.1 First-year ice and second-year ice

The difference in σ°s between first-year and second-year ice are shown in Fig 4.5 a-c for angles between 30° and 70°. It can be seen from these figures that the backscattering from first-year ice was lower than that from multiyear ice at 9.6 GHz, 13.6 GHz, and 16.6 GHz for like and cross polarizations. At 5.2 GHz however, the return from first-year ice at smaller angles of incidence was greater than that from second-year ice. This is possible because the surface of first-year ice may be rougher at the appropriate scale than that of second-year ice.

The contrast between first-year ice and second-year ice was greater than 5 dB at 60° for both like and cross polarizations. Because the feed used to measure the cross polarization at 9.6 GHz was damaged during the experiment, we could not be certain about the characteristics of the cross-polarized data. The cross-polarized data acquired at 40° and 50° seem abnormal, so no comparison can be made for those angles. The remaining results showed that the best contrast was given at 60° and 13.6 GHz. For the limited data, it cannot be shown that cross polarization gives significantly better contrast between first-year ice and second-year ice than like polarization.

Comparing Figure 4.5-b with the angular behavior of the contrast at 9.6 GHz and VV polarization at Mould Bay, October 1981, shown in Figure 4.5-a, we can see that the angular responses were similar ecept at 5.2 GHz. At that frequency the contrast increased less rapidly in the spring of 1983 than in the fall of 1981.

4.5.2 Lake Ice

Data for fresh-water lake ice were acquired at 9.6 GHz with vertical polarization. The angular behavior of σ° is shown in Figure 4.5-d. The lake ice had higher σ° than first-year ice. It gave σ° values similar to second-year sea ice, but with flatter slope. We are not in a position to make a definite statement regarding the apparent reasons for higher scattering because of the lack of ground truth data. **Although ground truth data were collected, the data were not made available to us, for unexplainable reasons.** It is possible that there were many air bubbles in the lake ice and/or a heavy snow cover was present on the lake ice that could produce

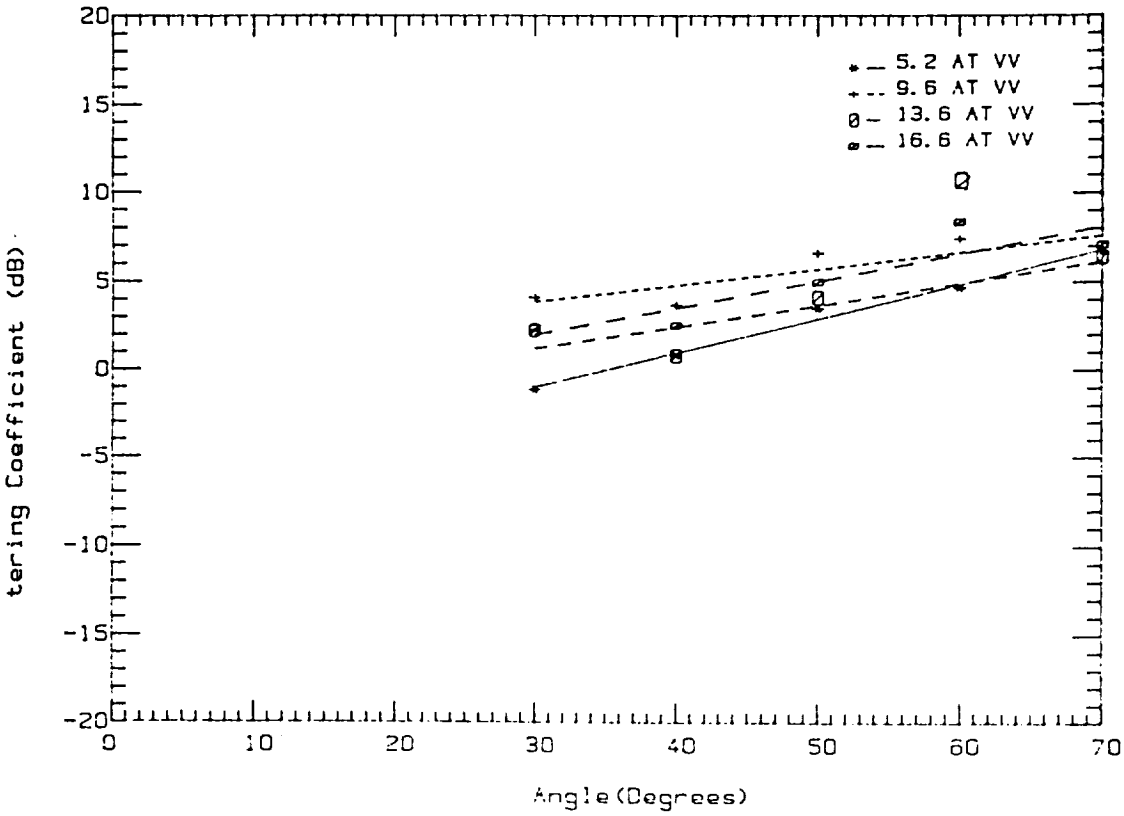

FIGURE 4.5-a. Contrast between FYI and SYI

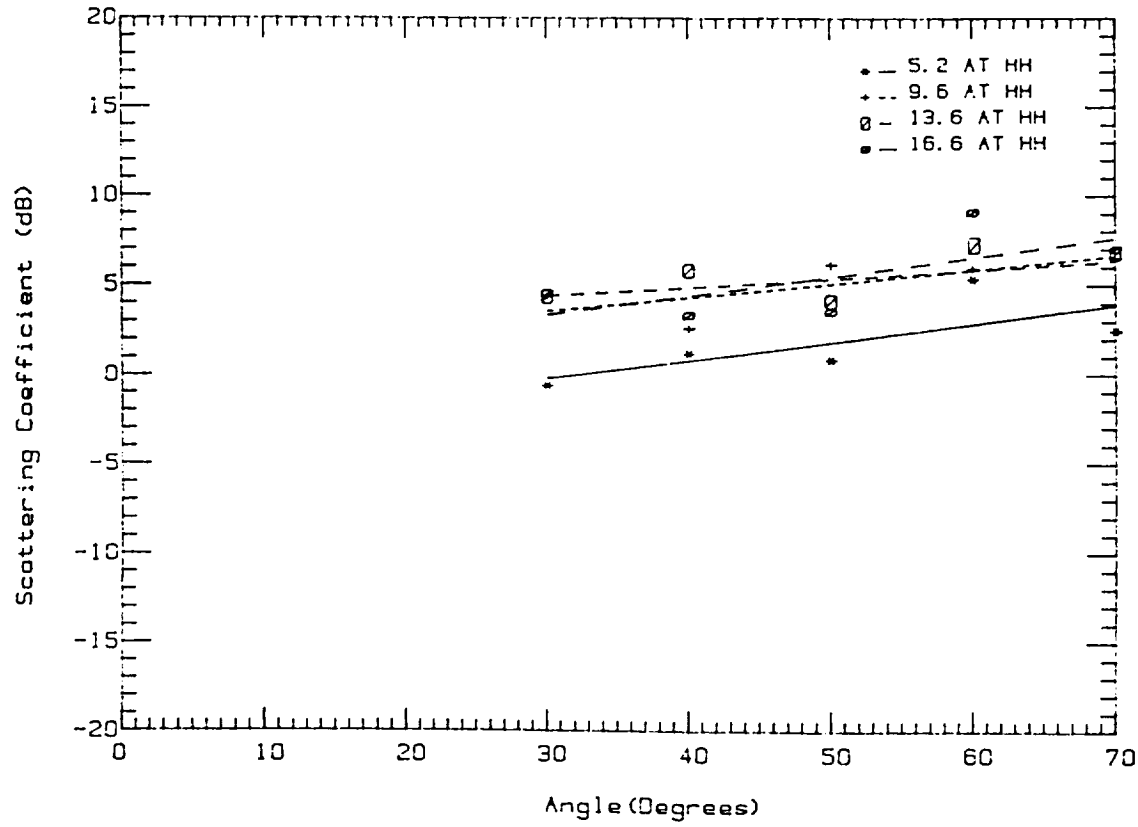

4.5-b. Contrast between FYI and SYI (1983)

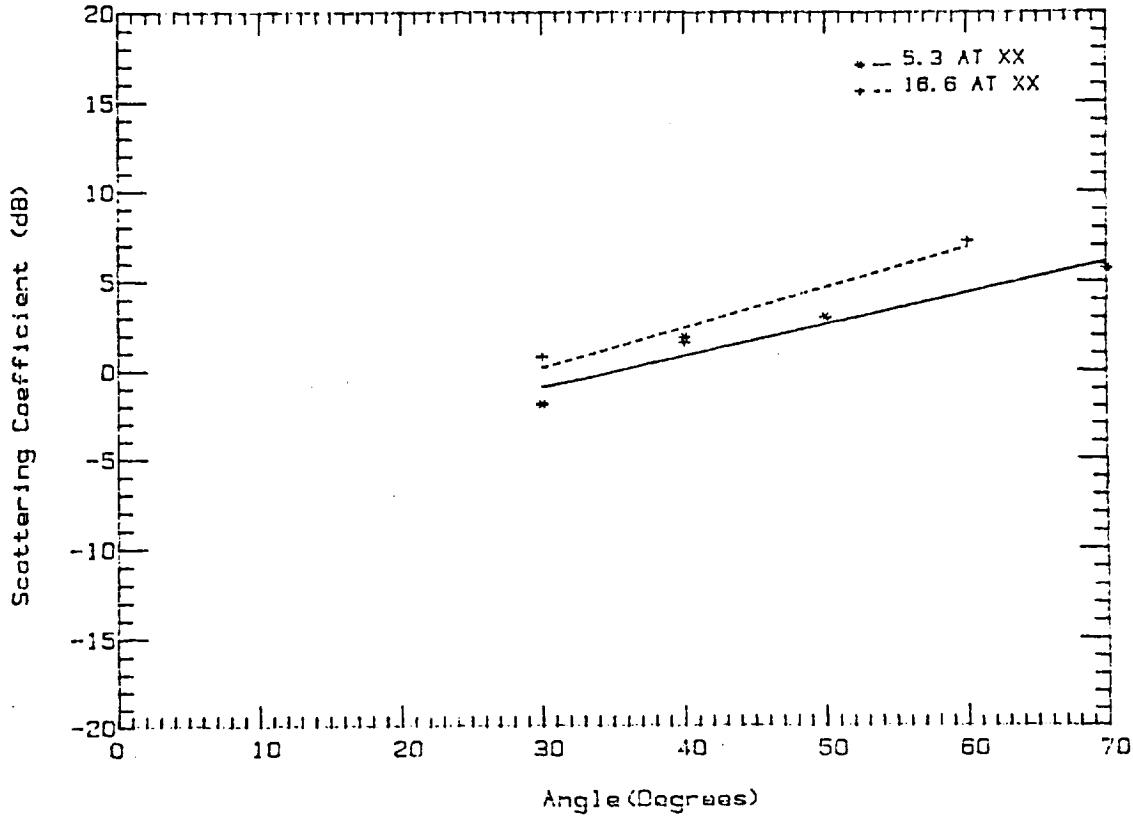

FIGURE 4.5-c. Contrast between FYI and SYI.

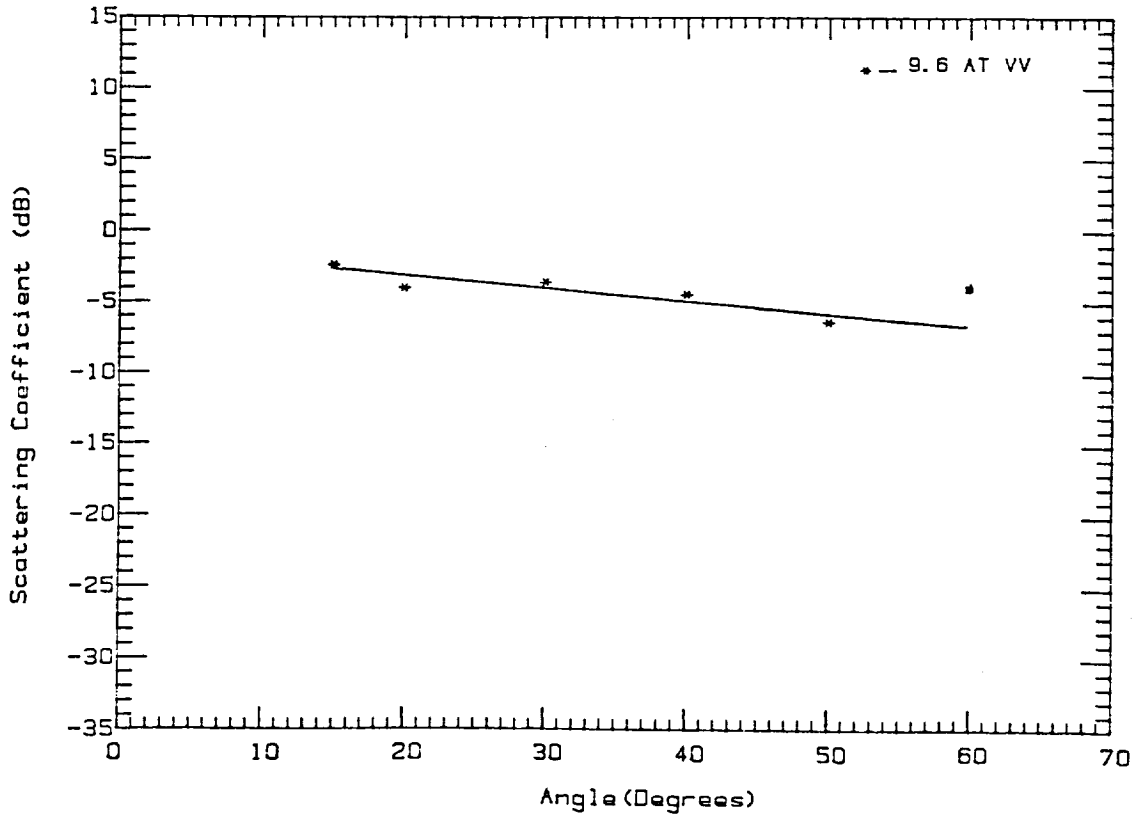

FIGURE 4.5-d. Mould Bay, Apr. 26, 1983 (Lake Ice)

enough volume scattering to raise σ° significantly, especially at large incidence angles. Moreover at 60° the average σ° was higher than 40° and 50°. This may be a local effect due to large snow drifts, since the footprints at the different angles do not coincide. Kim [1984] reported that at X-band the lake ice had higher σ° than first-year ice, as was observed here.

5.0 A METHOD FOR MEASURING SNOW DEPTH

5.1 Background

Although the Arctic is essentially dry, most of the precipation falls as snow, and snow cover of average depths ranging from 4 to 30 cm has been observed on first-year ice and multiyear ice. Snow cover alters the ice temperature profile and backscattering. During winter, snow effectively insulates the ice from cold polar air. An ice surface with snow cover is warmer than that without snow cover because thermal conductivity of snow is much lower than that of ice. Electromagnetic waves are attenuated in passing through the snow layer. Attenuation in dry snow is primarily from scattering, and absorption is usually negligible. Dry snow may increase the backscattered signal; the increase is more pronounced for smooth ice than for rough ice. Absorption is much higher than scattering in wet snow. The wet snow masks the return from ice surface.

Ulaby et al. [1982] developed a set of empirical equations for studying backscattering from snow-covered terrain. Kim [1984] modified and applied these equations to explain backscattering from snow-covered sea ice. He reported that dry snow cover of 5 cm or more will raise σ^o of smooth first-year ice by about 8 dB at 9 GHz. He also showed dry snow did not alter the scattering cross-sections of multiyear ice. Although these equations are suitable for investigating the effect of snow on sea ice qualitatively, they are not useful for estimating snow depth.

5.2 Fading Statistics

Fading complicates the measurement of a radar cross section of complex, area-extensive targets. Fading shows up as a rapid fluctuation in the received signals as the radar scans a target area. Figure 5.1 shows how fading affects the precision of the cross-section measurement. To construct a certain confidence interval around any scattering element, an assumption must be made about the statistics of the return power. Individual scattered signals vary about the mean by an amount described by the fading statistics.

For an area-extensive target containing a large number of scatterers of approximately equal backscatter amplitude, the assumption is made that the envelope of the backscattered voltage follows a Rayleigh probability density:

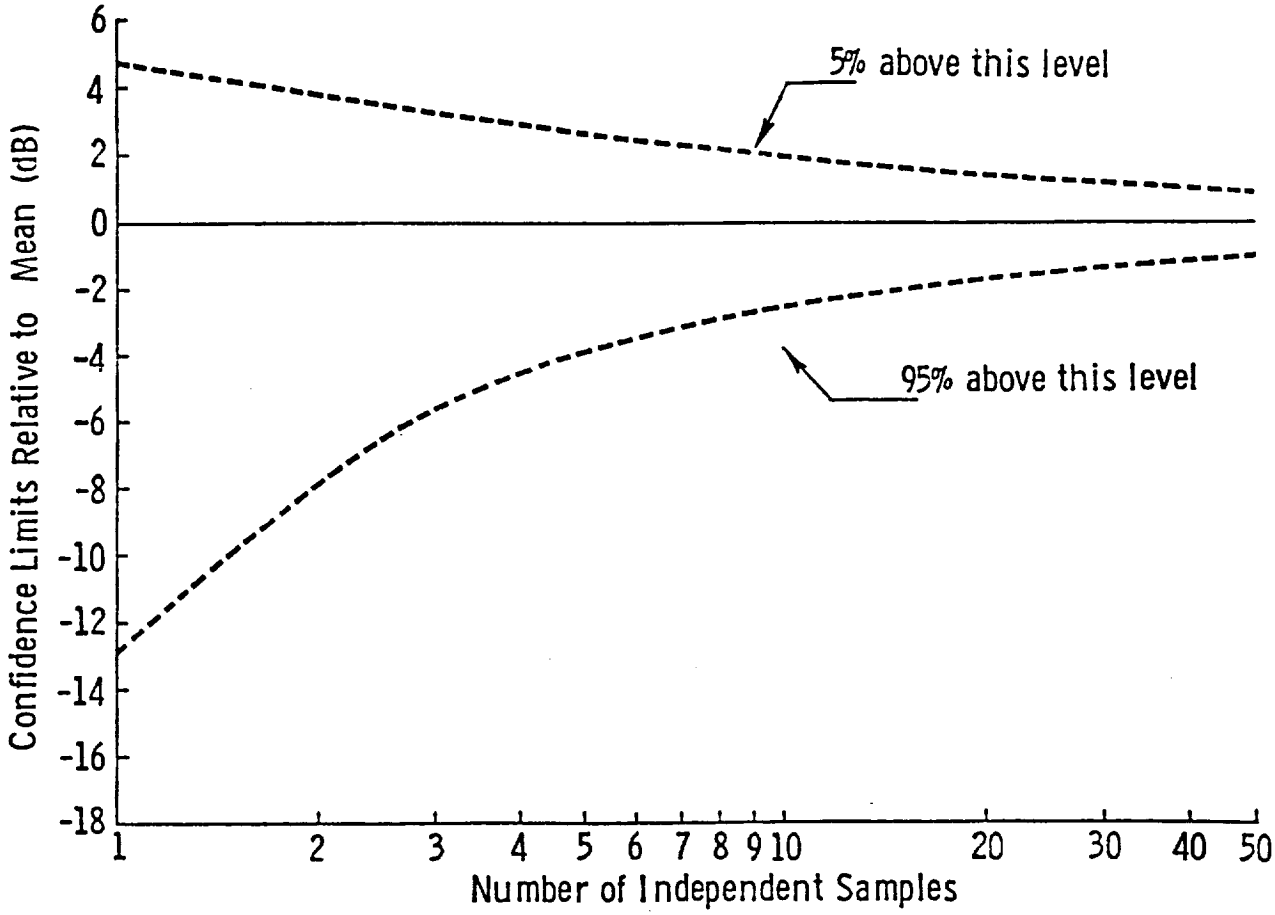

FIGURE 5.1. 90% Confidence interval for Rayleigh Distribution

$$P(V_e) = \frac{V_e}{\sigma^2} \exp\left[\frac{-V_c^2}{2\sigma^2}\right] \qquad (V_e > 0) \qquad (5.1)$$

Defining $W(t) = V(t)^2$, then the power has an exponential pdf:

$$P(W) = (1/2\ \sigma^2)\ \exp(-W/(2\sigma^2)) \qquad (5.2)$$

which is also a chi-square density function with two degrees of freedom. The chi-square density function with n degrees of freedom is defined as:

$$P_n(W) = \frac{1}{2^{n/2}\ \sigma^n\ \Gamma(\frac{n}{2})}\ \exp\left(-\frac{W}{2\sigma^2}\right) W^{n/2-1} \qquad (5.3)$$

Consider the average power, $\overline{W}$, of N samples, each distributed with an exponential distribution, that is,

$$\overline{W} = \frac{1}{N} \sum_{i=1}^{N} W_i \qquad (5.4)$$

Let

$$r = \sum_{i=1}^{N} Wi \qquad (5.5)$$

By the addition theorem of the chi-square distribution [Cramer,1946], we know the distribution of r will be chi-square distributed with 2N degree of freedom. Let n=2N, then:

$$P_{2N}(r) = \frac{1}{2^N \sigma^{2N}\ \Gamma(N)}\ e^{-\frac{\gamma}{2\sigma^2}}\ \gamma^{N-1} \qquad (5.6)$$

Finally we want to determine the density function of W, so define a new variable as $\bar{W} = r/N$; changing variables again we get:

$$P_{2N}(\bar{W}) = \frac{N^N}{2^N \sigma^{2N} \Gamma(N)} e^{\left(-\frac{N\bar{W}}{2\sigma^2}\right)} \bar{W}^{N-1} \qquad (5.7)$$

This is the Gamma density function of averaged power $\bar{W}$.

Now it can be seen that the expected density function of return power from a complex of discrete scatterers is chi-square distributed, and the parameter N refers to the actual number of independent samples averaged in frequency by a radar system within one look. The Rayleigh distribution for voltage or the chi-square distribution for power has been widely used for terrain surfaces and has been shown to provide good agreement with experimental results [deLoor, 1974].

5.3 The Method for Measuring Snow Depth

5.3.1 Calculation of the number of independent samples

Frequency averaging by the system reduces the uncertainty in the measurement due to fading. Because of the snow, more independent samples are involved than for the surface alone, with the additional number nearly proportional to the snow depth. It is therefore possible to evaluate the snow depth through determining the "extra" number of independent samples.

An FM-CW (or any other) radar may use excess bandwidth to obtain multiple independent samples in the range direction; and others are obtained by movement in the along-track direction. The number of independent samples is given by Ulaby, Moore and Fung [Chp. 8 & 11,1982]. The total number of independent samples due to frequency averaging is

$$N_f = N_r \cdot N_a \qquad (5.8)$$

where N_r is the number in the range direction, and N_a is the number in the azimuth direction.

The number of independent samples in the range direction is the ratio of the resolution actually used to that possible with the bandwidth used. This can be expressed as

$$N_r = B_r/B = r_r/r_{r\ \text{possible}} \qquad (B_r>B) \tag{5.9}$$

where r_r possible is the resolution that could be obtained with the bandwidth B_r that is actually used, and r_r is the actual resolution set by the antenna beamwidth. B is the bandwidth that would be needed to achieve r_r. The expression for B_r is [Waite, 1970]

$$B_r = 150/D \text{ MHz} \tag{5.10}$$

where D is the distance in meters between the scatterer located closest to the radar and the scatterer located farthest from the radar (as measured radially from the antenna).

For a flat target, with negligible penetration of the EM wave into the target, D is the same as the radar range resolution.

There are two expressions for D. If the range resolution is not limited by the bandwidth of the IF filter, then D is given by

$$D = R_{out} - R_{in} = H(\sec\theta_{out} - \sec\theta_{in}) \tag{5.11}$$

where

H = the height of the antenna

$\theta_{out} = \theta + \beta_{el}$

$\theta_{in} = \theta - \beta_{el}$

θ = the incidence angle

β_{el} = the effective elevation beamwidth

If the range resolution of the radar is determined by the bandwidth of the IF filter, then D is given by

$$D = R\, f'_{if} / f_{if} \tag{5.12}$$

where

R = the range of the target

f'_{if} = the bandwidth of the IF filter

f_{if} = the center frequency of the IF filter.

For the two cases of the range resolution D, the one that yields the smaller value should be used in the calculation of number of independent samples, that is

$$N_r = D/r_r \text{ possible} \tag{5.13}$$

where the subscript r indicates range direction.

In the along-track direction, the Doppler frequency is given by (see Fig. 5.2 for the geometry)

$$f_d = 2ux/R\lambda \tag{5.14}$$

where

u = the velocity of the sled-radar

x = the displacement from the side-looking position

λ = the wavelength

R = the slant range.

The maximum value taken by x within the beam is

$$x_{max} = \beta_h\, R/2 \tag{5.15}$$

where β_h is the horizontal antenna beamwidth. Substituting this value into

(5.14), we find that the maximum Doppler frequency is

$$f_{dmax} = 2u\beta_h/\lambda = - f_{dmin} \tag{5.16}$$

Note that this is also the magnitude of the minimum Doppler frequency f_{dmin}. Hence, the Doppler bandwidth associated with the sledscat radar is

$$f_d' = 2u\beta h/\lambda \tag{5.17}$$

Let the time for integrating the fading signal be T, and the number of independent samples in the along-track direction be N_a then [Ulaby, Moore and Fung, Chap. 7, 1982]

$$N_a = f_d' T \tag{5.18}$$

where the subscript a indicates along track direction.

5.3.2 The model for determining the number of independent samples in frequency

The snow-free and the snow-covered second-year ice in the Mould Bay 1983 Experiment were assumed to be area-extensive and to consist of a large collection of approximately equal-amplitude scatterers, so the chi-square distribution of (5.7) is applicable.

A non-parametric,(chi-square) test, which gives a measure for the deviation of the empirical distribution from the hypothesis distribution [Fisz,1958], is used for determining the distribution of the fading signals. For this purpose, the following process is necessary [Bevinton, 1969]:

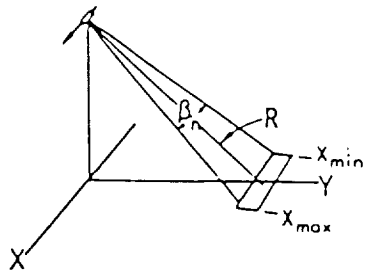

FIGURE 5.2. Geometry of SLAR fading

Define chi-square for the test as [Fisz, 1958]

$$\chi^2 = \sum_n (Q(n) - MP(n))^2 / MP(n) \qquad (5.19)$$

where

P(n) = the fitting model of the p.d.f.

M = the number of data points

Q(n) = the frequency for nth bin of the p.d.f.

and the 5% rule was used in this test.

(2) Find a reasonable bin size to minimize chi-square. (Referencing the empirical formula: # of data points $\simeq 2^k$, where k is the bin number).

(3) Try different numbers of independent samples to minimize the chi-square.

After determining the model parameter, the total number of independent samples in frequency, we see that for the nearly-bare ice data at the incident angle of 60°, 16.6 GHz and VV polarization (case A) and at 60°, 9.6 GHz and VV polarization (case B) according to (5.8) (assuming the speed u = 2.5 miles/hour) the calculation shows

The number of independent samples = 5.6 for case A

The number of independent samples = 7.1 for case B

and from the result of the best fitting [see Table 5.1]:

The number of independent samples = 5 for case A

The number of independent samples = 7 for case B.

A good match can be seen.

Table 5.1-a Data at 60°, 16.6 GHz, VV

# of pts	# of I.S.	D.O.F	chi-square	acceptable level
182	4	10	21.7	18.3
182	5	10	16.3	18.3
182	6	10	16.5	18.3
182	7	10	27.5	18.3

Table 5.1-b Data at 60°, 9.6 GHz, VV

# of pts	# of I.S.	D.O.F	chi-square	acceptable level
176	6	12	24.1	21.0
176	7	12	11.0	21.0
176	8	12	13.4	21.0
176	9	12	21.4	21.0

To test the model more precisely, recall the definition of the chi-square

$$\chi^2 = n \left(Q(n) - MP(n) \right)^2 / MP(n) \qquad (5.20)$$

If the model is correct, then

$$Q(n,M) / M \Longrightarrow P(n)$$

and [Lipsky, 1976]

$$Q(n, M) = P(n) + O(1/m^{1/2})$$

If the theory is true, when we vary the number of data points, the chi-square will not change significantly. On the contrary, if the theory is wrong, assuming the true model = P'(n) then

$$Q(n,M) = MP(n) + C(n)\sqrt{M} + \text{higher order terms} \tag{5.21}$$

where C(n) is the relative variance of the distribution.

and

$$Q(n,M) - MP(n) = M\,(P(n)'-P(n)) + C(n)\,M^{0.5} \tag{5.22}$$

Define R(n) = P(n)'-P(n), according to 5.22

$$\chi^2 = \sum_n (MR(n) - C(n)\,M^{0.5})^2/MP(n)$$

$$= M^n * (R(n) - C(n)/M^{0.5})^2/P(n) \tag{5.23}$$

The first term in Eq. 5.23 can be very large and the second term will be very small when M is increased. Now Eq. 5.23 can be written as

$$\chi^2 = M * \text{constant} \tag{5.24}$$

We conclude that if the theory is wrong, eventually when we make more measurements, χ^2 will be increased significantly.

For the snow-covered ice data (at 60°, 13.6 GHz and VV polarization) at first the same work was done as in the above section and 11 independent samples were obtained from the best fitting (see Table 5.2).

Table 5.2 Snow Data at 60°, 13.6 GHz, VV

# of pts	# of I.S.	D.O.F	chi-square	acceptable level
176	9	8	20.3	15.5
176	10	8	16.3	15.5
176	11	8	14.0	15.5
176	12	8	186.5	15.5

Then the 178 data points were divided into set A (containing the first 89 data) and set B (containing the remaining 89 data points). After processing the two sets we get consistent results (See Table 5.3) which tells that the model used is correct for the experimental data.

Table 5.3-a Data at 60°, 13.6 GHz, VV
(The first half of the data string)

# of pts	# of I.S.	D.O.F	chi-square	acceptable level
89	10	7	10.0	14.1
89	11	7	10.2	14.1
89	12	7	75.1	14.1

Table 5.3-b Data at 60°, 13.6 GHz, VV
(The second half of the data string)

# of pts	# of I.S.	D.O.F	chi-square	acceptable level
89	10	7	7.0	14.1
89	11	7	5.7	14.1
89	12	7	187.6	14.1

The calculation according to (5.8) shows that for surface only, the snow-covered data gives 7.2 independent samples yet the best fitting of the model provides 11 independent samples. The additional samples must from volume scatter by the snow.

The slant range through the snow d' may then be calculated as

d' = (Total number of independent samples--number of independent samples for surface) * (best range resolution in the snow) / (number of independent samples in azimuth) , N_a.

Considering refraction effect and assuming the dielectric constant of dry snow $\varepsilon = 1.7$ then

$$r_{r\ possible} = 0.20m,$$

Because $N_a = 1.6$,

$$d' = (11 - 7) * 0.20/1.6 = .50 \text{ meters}$$

Hence, converting from the slant range to vertical the snow depth is

$$d = 0.43 \text{ meters}$$

According to the investigators, during the Mould Bay April, 1983, experiment the average temperature was < = -5°C, (the snow was dry) and the snow depth was between 0.10 and 0.5 meters. A reasonable agreement can be seen; i.e.,the calculated depth is within the reported range. Specific information on snow depth for this path is unavailable.

6.0 CONCLUSIONS AND DISCUSSIONS

In this paper the Mould Bay 1983 spring experiment data were analyzed and comparisons were made with theory and with the Mould Bay 1981 fall experiment. The regression analysis indicates that a simple model ($\exp -\theta/\theta°$) represents the microwave backscatter data from sea ice well in the angular region 20°-70°. Higher frequencies and larger incidence angles seem from the data to be best suited to discriminate first-year ice from second-year ice. In accordance with mechanisms explained by Kim's theory, the microwave signature changed with ice age as predicted, but there was little difference between second-year and multiyear ice.

The like and cross polarizations are not independent; the depolarization ratio is a constant which is independent of frequency, incidence angle and ice types as indicated by the latest theory. All results from this experiment essentially confirm former experimental findings in sea-ice monitoring.

The method of measuring snow depth using a radar showed a reasonable match with experimental data. It seems that it should work with other snow-like media.

REFERENCES

Beckmann, P. and A. Spizzichino, The Scattering of Electromagnetic Waves from Rough Surfaces, New York: Pergamon Press, chap. 3, 1963.

Bevington R. Philip, Data Reduction and Error Analysis for the Physical Sciences, chap. 6 and chap. 11, 1969.

Bush, T. F., and F. T. Ulaby, "Fading Characteristics of Panchromatic Radar Backscatter from Selected Agricaltural Targets," IEEE Trans. Geosci. Electro., vol. GE-13, no. 4, pp. 149-157, October 1975.

Campbell, J. K., R. O. Ramseier, P. Gloersen, M. L. Bryan, "Microwave Remote Sensing of Sea Ice in th AIFJEX Main Experiment," Boundary Layer Meteorology, 13, pp. 309-337, 1978.

Eom, H. J., "Theoretical Scatter and Emission Models For Microwave Remote Sensing," Ph.D. Thesis, University of Kansas, Lawrence, Kansas, 1982.

Foldy, L. L., Phys.Rev. 67, 107 (1945).

Fung, A. K., "Character of Wave Depolarization by a Perfectly Conductuig Rough Surface and its Application to Earth and Moon Experiments," Plant. Space Sci, Vol. 15, pp.1337-1347, 1967.

Fung, A. K. and H. L. Chen, "On Backscattering From Two-Scale Rough Surfaces," AGARD Conference Proc.: Propagation Limitation in Remote Sensing, GP-90, pp. 1-13, 1971.

Fung, A. K. and H. J. Eom, "Note on the Kirchhoff Rough Surface Solution in Backscattering," Radio Science, vol. 16, no. 3, pp. 299-302, 1981.

Gogineni, S. P., "Theoretical Scatter and Emission Models For Microwave Remote Sensing," Ph.D. Thesis, University of Kansas, Lawrence, Kansas, 1984.

Lipsky, L. and J. D. Church, "Applications of a Queueing Network Model for a Computer System," Computing Surveys 9, 3 September 1977, 205-211, Marck Fisz, Probability and Mathematical Statistics, Ch. 9 and Ch. 12, 1961.

Moore, R.K., K. Soofi, and S.M. Purdusky, "A Radar Clutter Model: Averaged Scattering Coefficients of Land, Snow and Ice," RSL TR 2923-3, Remote Sensing Lab., University of Kansas, Lawrence, 1979.

Moore, R.K. and A.K. Fung, "Radar Determination of Winds at Sea," IEEE Proc., vol. 67, pp. 1504-1521, 1979.

Onstott, R.G., R.K. Moore, S.P. Gogineni, Y.S. Kim and D.B. Bushnell, "Helicopter-Borne Scatterometer," CRES Technical Report 331-24, The University of Kansas Center for Research, Inc., Lawrence, Kansas, 1982.

Roth, L.M.; Phys. Rev. B9, pp 2476, 1974.

Stiles, W.H., B.C. Hanson and F.T. Ulaby, "Microwave Remote Sensing of Snow - Experiment Description and Preliminary Results," Remote Sensing Laboratory Technical Report 340-1, University of Kansas Center for Research, Inc., Lawrence, Kansas, 1977.

Skolnik, M. I.; Introduction to Radar Systems, McGraw-Hill, New York, pp 80-97, 1980.

Tsang, L. and J.A. Kong, J. Appl. Phys., vol. 51, pp. 3450, 1980.

Tsang, L. and J.A. Kong, J. Appl. Phys., vol. 53, pp. 7162, 1982.

Ulaby, F.T., R.K. Moore and A.K. Fung, Microwave Remote Sensing, Addison-Wesley, Reading, Massachusetts, vol. II, ch. 11, 1982.

Ulaby, F.T., W.H. Stiles and M. Abdelrazik, "Snow Cover Influence on Backscatter From Terrain," Remote Sensing Laboratory Technical Report 527-2, University of Kansas Center for Research, Inc., Lawrence, Kansas, 1982.

Valenzuela, G.R., "Depolarization of EM waves by alightly rough surface," IEEE Trans. Ant. and Prop., vol. AP-15, no. 4, pp 552-557, 1967.

Kim, Y.S., R.K. Moore and R.G. Onstott, "Theoretical and Experimental Study of Radar Backscatter From Sea Ice," Remote Sensing Laboratory Technical Report 331-37, University of Kansas Center for Research, Inc., Lawrence, Kansas, January 1984.

Waite, W. P., "Broad-Spectrum Electromagnetic Backscatter," CRES Technical Report 133-11, The University of Kansas, Center for Research, Inc., Lawrence, Kansas, 1970.

Zhu, P.Y., A.K. Fung and K.W. Wong, "A Comparison Between Effective Medium Approximation and Quasicrystalline Approximation in Multiple Scattering Computation," Radio Science, vol. no. 3-4, 1987.

Zhu, P.Y., A.K. Fung and K.W. Wong, "Scattering of Electromagnetic Waves From a Half-Space of Randomly Distributed Discrete Scatterers and Polarized Backscattering Ratio Law," preprint, 1987.

Fung, A.K. and H.J. Eom, "Application of a Combined Rough Surface and Volume Scattering Theory to Sea Ice and Snow Backscatter," IEEE Trans. on Geoscience and Remote Sensing, vol. GE-20, no. 4, pp. 528-536, 1982.

Gray, L.J., "Microwave Remote Sensing of Sea Ice," Oceanography from Space Edited, J.F.R. Gower, Plenum Press, NY, pp. 785-799, 1980.

Gray, A.L., C.E. Livingstone, et al., "Simultaneous Scatterometer and Radiometer Measurements of Sea Ice Microwave Signatures," IEEE J. of Oceanic Engr., vol. OE-7, pp. 20-32, January, 1982.

Holtzman, J.C., Personal communication, 1987.

Kim, Y.S., "Theoretical and Experimental Study of Radar Backscatter From Sea Ice," PhD thesis, University of Kansas, Lawrence, 1984.

Kim, Y.S., R.K. Moore, R.G. Onstott and S.P. Gogineni, "Towards Identification of Optimum Radar Parameters for Sea-Ice Monitoring," Journal of Glaciology, vol. 31, no. 109, pp. 214-219, 1985.

Onstott, R.G., R.K. Moore and W.F. Weeks, "Surface-Based Scatterometer Results of Arctic Sea Ice," IEEE Trans. on Geoscience and Electronics, vol. GE-17, no. 3, pp. 78-85, 1979.

Onstott, R.G., R.K. Moore, S.P. Gogineni and C. Delker, "Four Years of Low-Altitude Broadband Backscatter Measurements," IEEE J. of Oceanic Engr., vol. OE-7, pp. 44-50, January, 1982.

Onstott, R.G. and S.P. Gogineni, "Active Measurements of Arctic Sea-Ice under Summer Conditions," Journal of Geophysical Research, vol. 90, pp. 5035-5044, May 20, 1985.

Parashar, S.K., "Investigation of Radar Discrimination of Sea Ice," PhD thesis, University of Kansas, Lawrence, 1974.

Ulaby, A.K., et al., "Microwave Remote Sensing: Active and Passive Vol. 2, Radar Remote Sensing and Surface Scattering and Emission Theory," Addison Wesley, Reading, MA, 1982.

Weeks, W.F., "Sea Ice: The Potential for Remote Sensing," Oceanus, vol. 4, no. 3, pp. 39-47, Fall 1981.

Gogineni, S.P., et al., "Intermediate Results of Radar Backscatter Measurements from Summer Sea Ice," Remote Sensing Laboratory Technical Report 3311-2, University of Kansas Center for Research, Inc., Lawrence, Kansas, July 1984.

APPENDIX I

AI.1. General Principle of FM-CW Radar

Figure A.1 shows a block diagram of a simple FM-CW radar system. For a given target at range R, the time that returned signals are delayed with respect to the transmitted signal is 2R/c. Using similar triangles it may be shown that

$$R = f_{if}c/4f_mB_r \qquad (A.1)$$

where

R = range to the target
f_{if} = center frequency of the band pass filter
C = speed of light
f_m = modulation rate
B_r = the RF bandwidth

In the Mould Bay 1983 experiment the height above the ground was determined by the height of the structure plus the additional component resulting from the length of the arm and the incidence angle θ. The total range to target R was calculated from the resultant height.

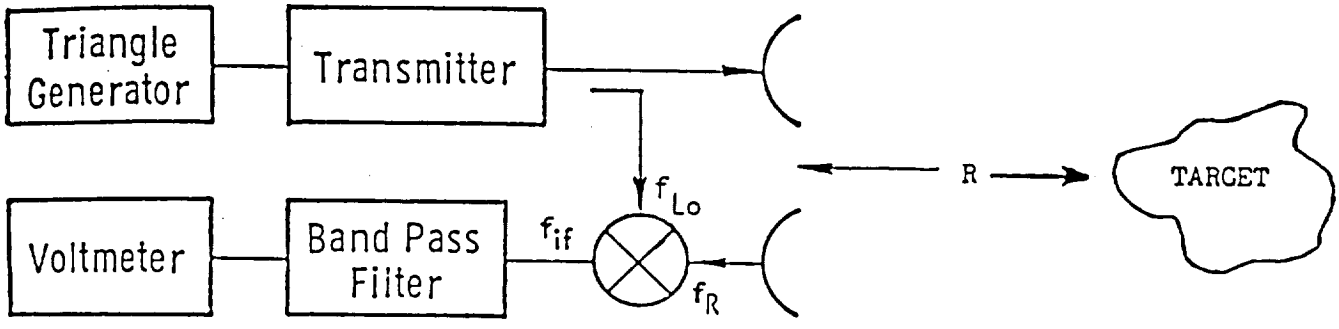

Figure A.1. Simple FM-CW Radar

The radar equation [Skolnik, 1980] relates the power received by the radar to the parameters of the target and the radar system, when the target whose physical area is small compared to the area illuminated by the main beam of the antenna. The radar equation is given by:

$$P_r = P_t \cdot G_t \cdot G_r \lambda^2 \sigma / (4\pi)^3 R^4 \qquad (A.2)$$

where

P_r = power received
P_t = power transmitted
R = the range to the target
G_r = gain of the receive antenna
G_t = gain of the transmit antenna
σ = the radar cross section of the target
λ = the signal wavelength

For an area-extensive target, σ varies with the area of the target that is illuminated by the radar, and the backscattering coefficient, σ° is the radar cross section per unit area, which is more useful than σ because it characterizes the target properties. The radar equation of an area-extended target is [Ulaby, Moore and Fung, 1982]:

$$P_r \frac{P_t \lambda^2}{(4\pi)^3} \int_{A_{ill}} \frac{G_r G_t \sigma^0}{R^4} \, dA \qquad (A.3)$$

where

A_{ill} is the area illuminated by the main beam of the antenna

From this equation, it can be seen that the contribution of backscattered energy from each incremental area is a function of the generally non-constant factors within the integral. For a high-gain antenna looking at a homogeneous target, Eq. A.3 can be approximated by

$$P_r \frac{P_t \lambda^2 \sigma^0}{(4\pi)^3 R^4} \int_{A_{ill}} G^2 dA \qquad (A.4)$$

Now assuming that the antenna has constant gain over its 3-dB product beamwidth, given by the maximum gain G_o, and a gain of zero outside this region, the radar equation can be written as

$$P_t = \frac{P_t G_o^2 \lambda^2 \sigma^0 A_{ill}}{(4\pi)^3 R^4} \qquad (A.5)$$

where A_{ill} is the area illuminated by the idealized antenna. A discussion of the errors associated with the perfect antenna approximation and the simplified integral are given in Ulaby, Moore and Fung, [1982].

AI.2. Determination of Backscattering Coefficient σ^o

The return power from a radar can be measured directly by a square-law detector. Calculating σ^o involves comparing with the magnitude of the power received from a calibration target with known radar cross section. This comparison must account for range and illuminated-area differences between the unknown target and the calibration target. The known target used to calibrate this system is a Luneberg lens reflector. Short-term gain variations are removed from the data by periodically replacing the antenna with a delay line during the measurements.

When sensing a target where the radar parameters remain essentially unchanged from one part of the resolution cell to the other, the detected power, P_t can be related to the returned power as

$$P_t = K_t^2 \left[\frac{P_t G_t G_r \lambda^2 \sigma^0 A_{ILL}}{(4\pi)^3 R_t^4} \right] \qquad (A.6)$$

where

R_t is the range to target

A_{ill} is the area illuminated by the idealized antenna

K_t is the system transfer constant which represents the effects of the receiver gain as well as the attenuation and conversion losses between antenna and radar

Shortly before or after recording the return from the target of interest, the delay line is switched into the system, replacing the antennas. If the delay line has loss L then the above equation can be written as:

$$P_{DLT} = K_t^2 P_t L \tag{A.7}$$

The ratio of Eq. A.6 and Eq. A.7 yields:

$$\frac{P_t}{P_{DLT}} = \frac{G_t G_r \lambda^2 \sigma^0 A_{ILL}}{(4\pi)^3 R_t^4 L} \tag{A.8}$$

Note that the ratio is independent of K_t or P_t.
When the target is a Luneberg lens, the measured power is

$$P_{LENS} = K_c^2 \left[\frac{P_t G_t G_r \lambda^2 \sigma_{SRT}}{(4\pi)^3 R_c^4} \right] \tag{A.9}$$

where

R_c is range to the Luneberg Lens
K_c is the system transfer constant at the time of the lens
σ_c is the cross section of the lens

A delay line reading is also made at this time and the output is given by

$$P_{DLL} = K_c^2 P_t L \tag{A.10}$$

and the ratio of Eq. 2.9 and Eq. 2.10 is

$$\frac{P_{LENS}}{P_{DLL}} = \frac{G_t G_r \lambda^2 \sigma_{SRT}}{(4\pi)^3 R_c^4 L} \tag{A.11}$$

Combining equation (A.11) and (A.8) results the following expression for σ° in dB:

$$\sigma^\circ(dB) = P_t(dB)-P_{LENS}(dB)-P_{DLT}(dB)+P_{DLL}(dB) + 40\log(R_t/R_c)+\sigma_c(dB)-10\log A_{ill} \quad (A.12)$$

where $P_t(dB)$, $P_{LENS}(dB)$, $P_{DLT}(dB)$, $P_{DLL}(dB)$ are measured and recorded at the time of the experiment

AI.2.1 Illuminated Area

The illuminated area is determined using the geometry shown in Figure A.2. The footprint of a radar beam is a skewed ellipse on the ground. The area A_{ILL} of the ellipse is calculated as:

$$A_{ill} = (\tfrac{1}{2} \text{ major axis})(\tfrac{1}{2} \text{ minor axis})\pi \quad (A.13)$$

From the geometry of Figure A.2, expressions for the two axes are

$$M_{maj} = R_t\cos\theta\left[\tan(\theta + \beta_E/2) - \tan(\theta - \beta_E/2)\right] \quad (A.14)$$

$$M_{min} = 2R_t \tan(\beta_A/2) \quad (A.15)$$

and

$$A_{ILL} = (\pi/2)R_t^2 \cos\theta\cdot\tan(\beta_A/2)\cdot\left[\tan(\theta + \beta_E/2) - \tan(\theta - \beta_E/2)\right] \quad (A.16)$$

where

M_{maj} = major axis
M_{min} = minor axis
R_t = range to target
θ = pointing angle of antennas off vertical
β_e = effective gain product beamwidth in the elevation plane
β_a = effective gain product beamwidth in the azimuthal plane

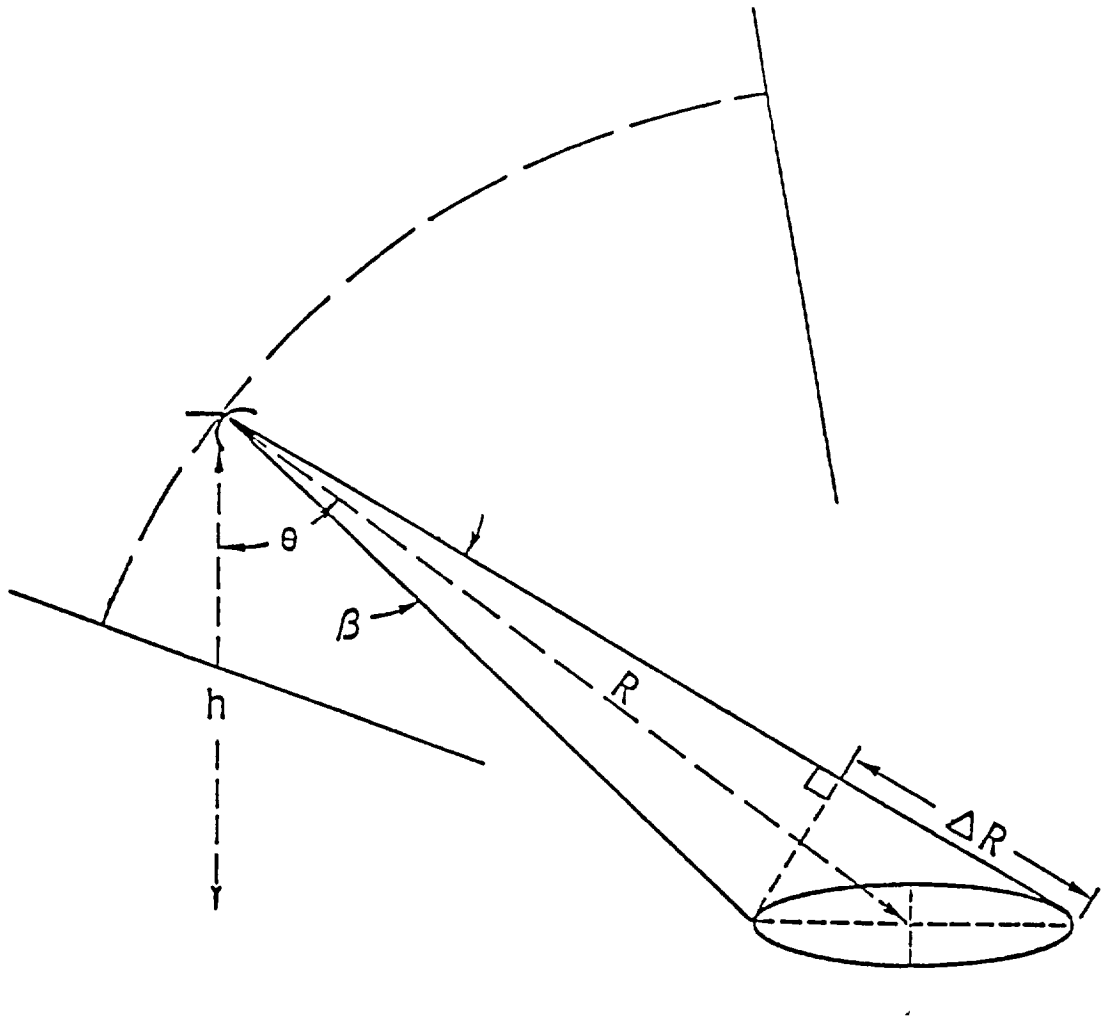

Figure A.2. Parameters Used in Illuminated Area Calculations

If the range is limited by the IF bandpass filter, the calculation may be divided into three cases according to the reduction of the illuminated area by the filter. The details are given in Onstott et al. [1982].

APPENDIX I-A

Mould Bay Apr. 1982 Experiment Data (13 = FYI, 19 = MYI, 99.99 = Missing)

TYPE V13VV

GHZ	ANG=15	ANG=20	ANG=30	ANG=40	ANG=50	ANG=60	ANG=70	ANG=80
5.2	99.99	-7.66	-15.35	-17.84	-19.39	-22.68	-25.48	-24.94
9.6	-4.31	-2.36	-7.85	-10.52	-15.57	-15.76	-19.61	99.99
13.6	0.70	0.25	-2.93	-4.36	-9.08	-12.74	-12.86	99.99
16.6	0.72	0.18	-1.22	-1.90	-3.54	-9.00	-10.95	99.99

TYPE V13HH

GHZ	ANG=15	ANG=20	ANG=30	ANG=40	ANG=50	ANG=60	ANG=70	ANG=80
5.2	99.99	-5.89	-13.91	-17.71	-18.19	-24.13	-25.02	-25.68
9.6	-4.04	-5.48	-7.19	-10.75	-15.00	-14.08	-16.64	-20.42
13.6	0.12	-2.48	-5.65	-10.39	-11.35	-11.13	-14.55	-15.55
16.6	0.99	-0.86	-3.95	-3.13	-6.88	-12.15	-10.76	-8.15

TYPE XXV13XX

GHZ	ANG=15	ANG=20	ANG=30	ANG=40	ANG=50	ANG=60	ANG=70	ANG=80
5.2	99.99	-22.78	-23.32	-26.72	-27.52	-31.34	-31.81	99.99
9.6	-10.76	-12.84	-11.25	-12.34	-17.91	-21.87	99.99	99.99
13.6	-10.06	-11.20	-13.62	-20.76	-21.74	-20.87	99.99	99.99
16.6	-6.88	-8.00	-4.61	-4.67	-5.89	-13.84	99.99	99.99

TYPE V19VV

GHZ	ANG=15	ANG=20	ANG=30	ANG=40	ANG=50	ANG=60	ANG=70	ANG=80
5.2	99.99	-9.95	-16.50	-17.03	-15.90	-18.02	-18.76	-20.12
9.6	99.99	0.51	-3.79	-6.88	-8.97	-8.36	-12.71	-11.41
13.6	99.99	3.91	-0.73	-3.60	-4.97	-1.74	-6.50	-11.03
16.6	99.99	6.35	1.10	0.59	1.43	-0.64	-3.88	-5.93

TYPE V19HH

GHZ	ANG=15	ANG=20	ANG=30	ANG=40	ANG=50	ANG=60	ANG=70	ANG=80
5.2	99.99	-9.54	-14.55	-16.50	-17.34	-18.60	-22.54	-19.43
9.6	99.99	1.63	-2.90	-8.15	-8.86	-8.15	-10.14	-14.42
13.6	99.99	6.05	-1.33	-4.60	-7.24	-5.26	-7.81	-13.44
16.6	99.99	2.21	0.56	0.18	-3.34	-3.06	-3.77	99.99

TYPE V19XX

GHZ	ANG=15	ANG=20	ANG=30	ANG=40	ANG=50	ANG=60	ANG=70	ANG=80
5.2	99.99	-26.75	-25.14	-24.78	-24.53	-23.66	-26.08	-23.90
9.6	99.99	-9.57	-10.50	-11.30	-16.59	-16.01	-19.71	-20.17
13.6	99.99	-9.52	-12.49	-11.01	-11.42	-11.76	-14.40	-14.43
16.6	99.99	-3.69	-3.78	-3.07	-7.11	-6.61	-10.21	-8.18

APPENDIX II

AII.1. Profile data processing

To get the returned-power profile plots, the following procedures were used: (1) Use program ND-MB.bas to dump data files from tape to disk and use program H2D.bas to convert data from hexidecimal to decimal. (2) Identify each run number and put files in correct order; then program MG.bas merges files to obtain consistent series of data in distance. Use program IV-MB.bas to reverse the output from step (1) if needed. (3) Run program CV-MB.bas to convert raw data to power in dB. (4) Finally, use program NP-MB.bas to plot output from step (3).

AII.2. σ° processing

The formula for calculating σ° is based on Equation A.12. The σ_{LENS} numbers are standard values of a Luneberg-lens radar target used during the radar calibration. The DLL readings are an average of the readings taken during lens measurements. DLT readings were the readings taken during target measurement. The DLT values were updated when processing the data. The R_c was obtained during lens measurements and the R_t was computed according to incidence angle. The illuminated area is determined from known beamwidths, incidence angles and the antenna height. Since the illuminated area at large incidence angles can be very large, a range filter was used in the receiver to limit the area.

After running the file-merging routine MG-MB.bas, described in section 1, a program called COMBN.bas was used to combine the raw signals with the master file which contains the calibration data and needed radar operation parameters into a single file. A program called MBS1.for was developed to calculate average backscattering coefficient σ° and convert them to dB. Upon completion of MSS1.for, another program SEP-MB.pas was developed to sort the σ° values for like conditions (polarizations, frequencies, and angles). Finally, the program FREQRESP-.bas and ANGLRESP.bas were used to plot frequency and polarization response curves.

AII.3. Statistical data processing

The procedures of processing data for statistical tests are outlined as follows: (1) Program HIST.pas was used to plot histograms so that the trends of raw data distribution could be examined, and (2) Program "MBFIT.bas" was developed to verify a non-parametric hypothesis and find best fitting parameters to describe a x^2 [2N] distribution.